Brigham Young University
BYU ScholarsArchive

All Theses and Dissertations

2012-12-12

Investigation of Low-Stress Silicon Nitride as a Replacement Material for Beryllium X-Ray Windows

David B. Brough
Brigham Young University - Provo

Follow this and additional works at: https://scholarsarchive.byu.edu/etd

 Part of the Astrophysics and Astronomy Commons, and the Physics Commons

BYU ScholarsArchive Citation

Brough, David B., "Investigation of Low-Stress Silicon Nitride as a Replacement Material for Beryllium X-Ray Windows" (2012). *All Theses and Dissertations*. 3402.
https://scholarsarchive.byu.edu/etd/3402

This Thesis is brought to you for free and open access by BYU ScholarsArchive. It has been accepted for inclusion in All Theses and Dissertations by an authorized administrator of BYU ScholarsArchive. For more information, please contact scholarsarchive@byu.edu, ellen_amatangelo@byu.edu.

Investigation of Low Stress Silicon Nitride as a Replacement Material for Beryllium in X-ray Windows

David Brent Brough

A thesis submitted to the faculty of
Brigham Young University
in partial fulfillment of the requirements for the degree of

Master of Science

Robert Davis, Chair
Richard Vanfleet
David Allred

Department of Physics and Astronomy

Brigham Young University

December 2012

Copyright © 2012 David Brough

All Rights Reserved

ABSTRACT

Investigation of Low Stress Silicon Nitride as a Replacement Material
for Beryllium in X-ray Windows

David Brent Brough
Department of Physics and Astronomy, BYU
Master of Science

The material properties of low stress silicon nitride make it a possible replacement material for beryllium in X-ray windows. In this study, X-ray windows made of LPCVD deposited low stress silicon nitride are fabricated and characterized. The Young's modulus of the LPCVD low stress silicon nitride are characterized and found to be 226±23 GPa. The residual stress is characterized using two different methods and is found to be 127±25 MPa and 141±0.28 MPa.

Two support structure geometries for the low stress silicon nitride X-ray windows are used. X-ray windows with thicknesses of 100 nm and 200 nm are suspended on a silicon rib support structure. A freestanding circular geometry is used for a 600 nm thick X-ray window.

The 100 nm and 200 nm thick low stress silicon nitride X-ray windows with a silicon support structure are burst tested, cycling tested and leak rate tested. The average burst pressure for the 100 and 200 nm films on a silicon support structure are 1.4 atm and 2.2 atm respectively. Both 100 nm and 200 nm windows are able to withstand a difference in pressure of 1 atm for over 100 cycles with a leak rate of less than 10^{-10} mbar-L/s.

The low stress silicon nitride with 100 nm and 200 nm thicknesses, the 600 nm freestanding low stress silicon nitride windows and freestanding 8 micron thick beryllium windows are mechanical shock resistance tested. The support structure low stress silicon nitride and beryllium windows are tested with an applied vacuum. The freestanding 600 nm thick low stress silicon nitride windows burst at 0.4 atm and are therefore mechanical shock wave tested without an applied vacuum.

The support structure low stress silicon nitride windows fractured when subjected to an acceleration of roughly 5,000 g. The 8 micron thick beryllium windows are subjected to accelerations of over 30,000 g without fracturing. A quasistatic model is used to show that for low stress silicon nitride with a freestanding circular geometry, an acceleration of 10^6 g is required to have the same order of magnitude of stress caused by a pressure differential of 1 atm. Low stress silicon nitride can act as a replacement for beryllium in X-ray windows, but the support geometry, residual stress, and strength of the material need to be optimized.

Keywords: low stress silicon nitride, x-ray windows, beryllium, shock test, thin-film characterization

ACKNOWLEDGMENTS

Thank you, Dr. Davis, for your patience, direction, guidance and support throughout the research process. Thank you, Dr. Vanfleet, Dr. Sterling Cornaby and Steven Liddard, for your direction and support on this project. Thank you, Lawrence Barrett for your assistance in the mechanical shock testing and apparatus design.

Most of all, thank you to my wife Kendree for being willing to sacrifice so that I can fulfill this dream. I could not have done it without you.

TABLE OF CONTENTS

LIST OF FIGURES

LIST OF TABLES

COMMON ACRONYMS

low stress silicon nitride (LSSN)
low pressure chemical vapor deposition (LPCVD)
potassium hydroxide (KOH)
reactive ion etching (RIE)

Chapter 1

Introduction

1.1 The Basic Functionality of X-ray Windows

Most X-ray detectors need to be in a vacuum environment to function. Therefore, X-ray windows serve two purposes:

- The windows allow X-rays into the vacuum chamber which contains the detector, so the x-rays can be detected. The windows have to be a very thin foil or membrane in order for soft x-rays (under 2 keV) to penetrate.
- The X-ray windows have to be strong enough to hold off 1atm of pressure and also be impermeable to gas. Detectors are in sealed modules, so if the windows are permeable to gas, the vacuum surrounding the detectors degrades.

The two functions of x-ray windows are often at odds with each other. On one hand X-ray transmission increases as the thickness of the membrane decreases, and on the other hand physical strength increases as the window thickness increases. The challenge with designing and building of x-ray windows is both these conflicting purposes need to be satisfied.

1.2 X-ray Spectroscopy and Transmission

X-rays can be used to excite or eject atomic core electrons. The hole created by the excitation of the core electron is filled by an electron from an outer shell of the atom. X-rays are emitted when the electrons transfer to lower energy states. The energies of the emitted X-rays are unique to the atom and provide a method for identification of elemental compositions in samples. This method of analysis is referred to as atomic core-electron spectroscopy [1]. X-ray windows

are important technology that is used to improve elemental analyses in many applications, including microscopy, mining, consumer product screening, and scrap metal identification.

The classification of the X-rays used in atomic core-electron spectroscopy is soft X-rays. Soft X-rays interact strongly with low Z elements, and as a result can also be absorbed within a few centimeters of air in ambient conditions [4]. In hand held devices that use X-ray spectroscopy, the sample remains in air and X-ray windows are used to keep the X-ray source and detector in a vacuum. An ideal X-ray window is thin enough to allow for soft X-ray transmission, but can handle the stresses required to maintain a pressure differential of one atmosphere on the other side. The vacuum on one side of the window allows the soft X-rays to travel between the window and the X-ray source or detector with little attenuation.

X-ray transmission properties of materials have been modeled previously [4] [13]. The model assumes that X-ray absorption occurs with atoms that are not interacting with each other in the solid. This assumption is reasonable except at an absorption edges. The transmission can be modeled with equation 1-1.

$$T = e^{-n\mu_a H} \tag{1-1}$$

In equation 1-1, H is the thickness of the material, n is the index of refraction, and μ_a is the photoabsorption cross section and can be determined by the equation 1-2.

X-ray transmission is exponentially dependent on thickness, H, as shown in equation 1-1 and is a parameter that can be manipulated. The photoabsorption cross section, μ_a, and the index of refraction, n, can also be manipulated by changing the material. Thin films made from low Z elements transmit soft X-rays with less attenuation than thin films of the same thickness made with high Z elements. This is due to the increase in the photoabsorption cross section of elements with more electrons [43].

1.3 X-ray Window Materials

Some examples of materials that have been used to make X-ray windows are beryllium, silicon, silicon nitride, boron nitride, silicon carbide, as well as polymer membranes (all of which are low Z compounds). As stated before, if the thickness of the X-ray window decreases the X-ray transmission increases. Therefore the mechanical properties such as Young's modulus, Poisson's ratio, residual stress, and tensile strength of thin films comprised of low Z elements need to be understood to make X-ray windows as thin as possible, while still being able to hold vacuum.

The most common material used to make X-ray windows is beryllium. Thin films of beryllium can be made relatively thick and still be transparent to soft X-rays because of its low Z number. One disadvantage to using beryllium is that if broken, beryllium dust is toxic [18] [20]. One non-toxic material that could be used as a replacement for beryllium is low stress silicon nitride (LSSN). It also has a relatively low Z number and has a low residual stress. In this study the Young's modulus, residual stress, and tensile strength of LSSN thin films are characterized. Mechanical integrity window tests such as mechanical shock resistance test, bulge test, burst test, cycling test and leak rate test are also done. LSSN with and without a silicon support structure are also compared in order to evaluate the possibility of replacing beryllium as an X-ray window material.

1.4 Computed X-ray Transmission Curves

Computed X-ray transmission curves were generated using the database information provided by the Center of X-ray Optics. The material, thickness, and density were given and the transmission percentages as a function of energy were produced. X-ray transmission curves were created for beryllium and stoichiometry silicon nitride both with and without, a silicon support

structure between the energy range of 100 to 10,000 eV and can be found in figures 1-2 and 1-1 respectively.

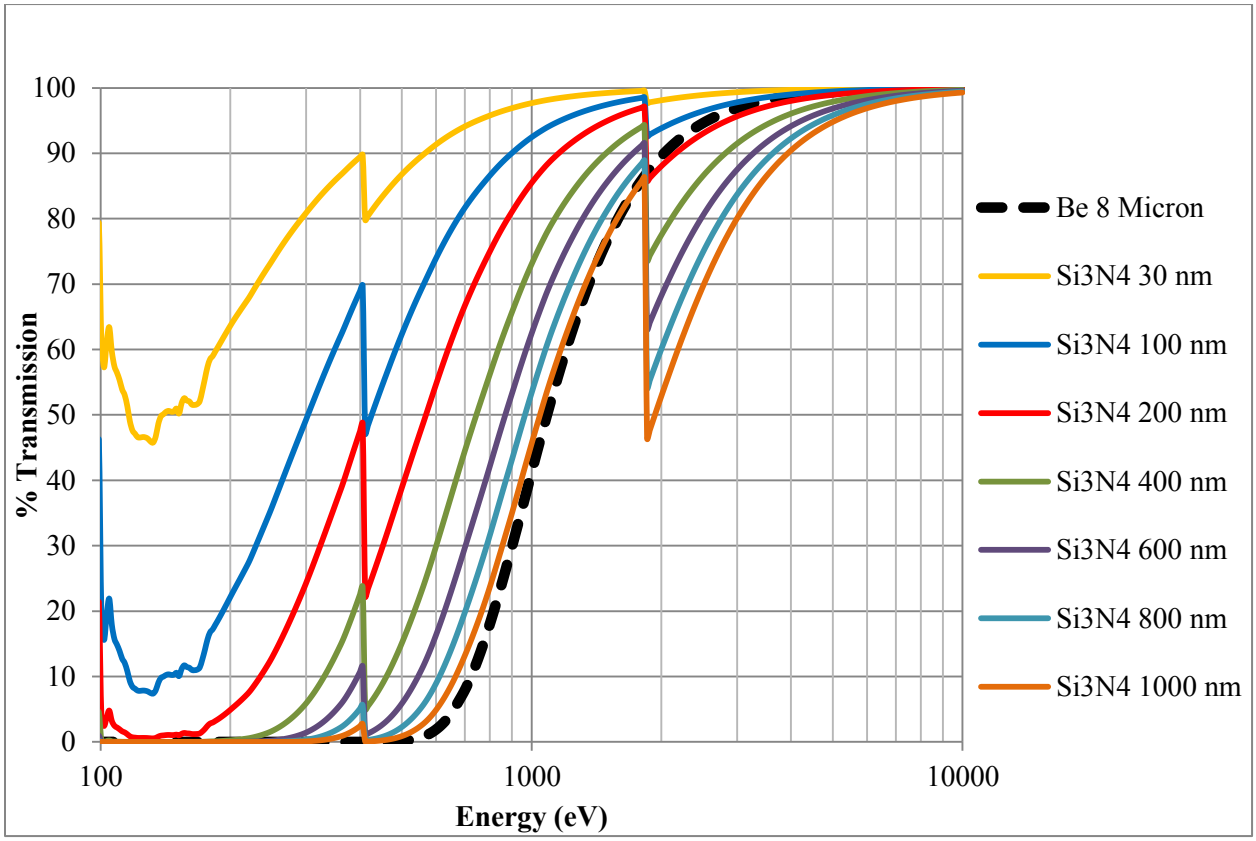

Figure 1-1 Computed X-ray transmission curves for silicon nitride and beryllium with freestanding geometries using data provided by the Center of X-ray Optics database

Computed X-ray transmission curves were created for stoichiometric silicon nitride without a support structure for a thickness varying from 30 nm to 1 micron and compared with the theoretical X-ray transmission curve of eight micron thick beryllium without a support structure. These curves can be found in figure 1-1. The two absorption edges found in the silicon nitride curves at 1839 eV and 402 eV are due to the K edges for silicon and nitrogen respectively.

In comparing the X-ray transmission curves found in figure 1-1, all of silicon nitride has higher percentages of X-ray transmission than the beryllium window in the energy range below

the silicon absorption edge. In the energy region above the silicon absorption edge, only the curves that were less than 200 nm thick outperformed the 8 micron beryllium. All the LSSN windows and the beryllium window have nearly 100% transmission above 10k eV.

X-ray transmission curves for silicon nitride with thicknesses of 100 nm and 200 nm on a silicon support structure were also compared to the X-ray transmission curve for 8 micron thick beryllium without a support structure. These curves can be found in figure 1-2. With the silicon support structure the silicon nitride windows are expected to have superior X-ray transmission performance compared to 8 micron beryllium windows below roughly 1450 eV, but the beryllium should have higher X-ray transmission above 1450 eV.

The model used to generate X-ray transmission curves assumes that the atoms in the solid are not interacting with each other [4] [13]. This of course is not true. The energies of the interatomic bonds can have an effect on the X-ray transmission around the absorption edges. Over a large energy range the curves provide a general understanding of a material's X-ray transmission performance, but if energies near an absorption edge require a high amount of accuracy other models would need to be used.

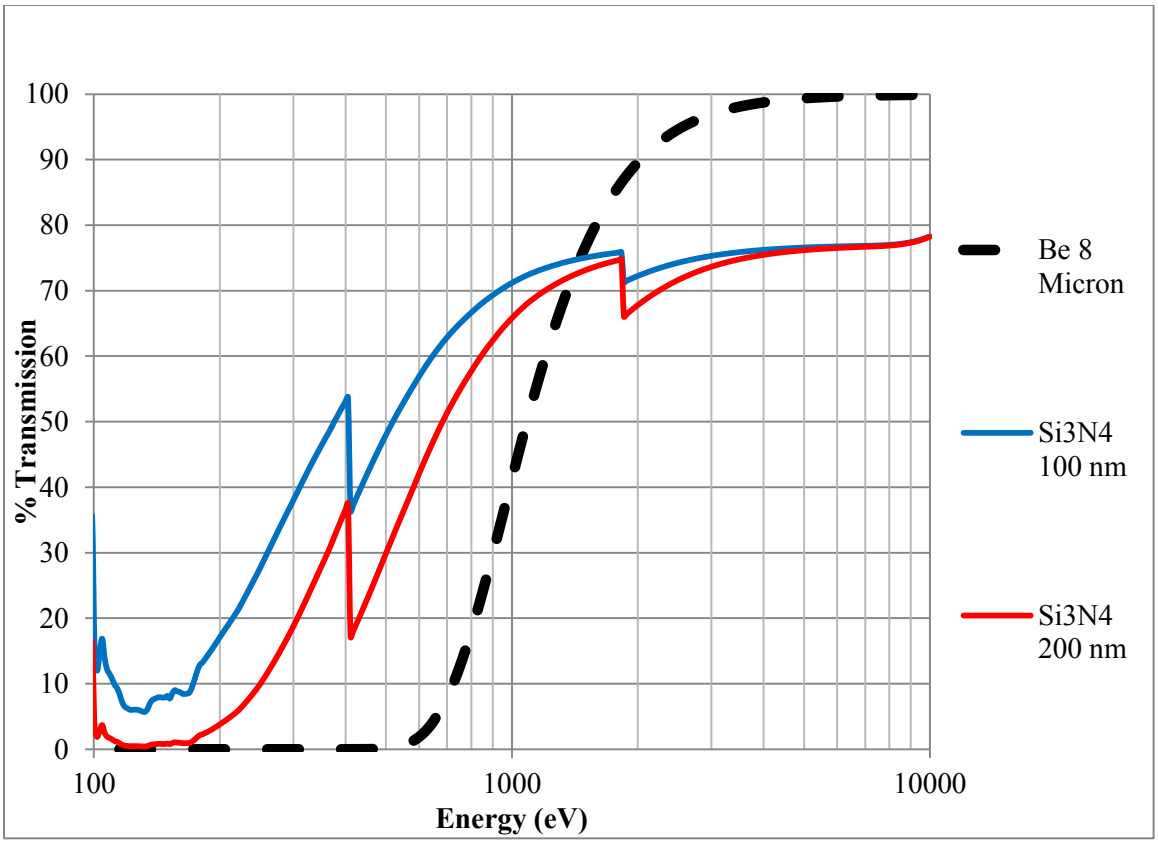

Figure 1-2 Computed X-ray transmission curves for beryllium with a freestanding geometry and silicon nitride with silicon support structure using data provided by the Center of X-ray Optics database

In this study the thicknesses of LSSN on a support structure were chosen to be 100 nm and 200 nm. For the freestanding geometry, the thicknesses of LSSN were chosen to be 400 nm and 600 nm. These thicknesses should have X-ray transmission performances similar to 8 micron beryllium X-ray windows.

1.5 Low Stress Silicon Nitride and Beryllium X-ray Windows

In this study LSSN X-ray windows are compared to 8 micron thick beryllium windows provided by Moxtek Inc. LSSN windows with a silicon support structure and freestanding geometries are fabricated.

A comparison between the X-ray windows is done by completing a series of tests on the LSSN and comparing those results to results from tests done previously on beryllium X-ray windows. These tests include burst, cycling and leak rate tests. The mechanical shock resistance is tested for both the LSSN and beryllium windows, which had previously never been established for beryllium windows. The mechanical shock resistance testing is done using a pendulum apparatus.

1.6 Properties of Low Stress Silicon Nitride

LSSN is used in a variety of applications including ball bearings for mechanical systems, a diffusion barrier, a passivation layer, a dielectric material, X-ray masks, X-ray windows, etch mask, and etch stop [2][3][6][23]. LSSN is an amorphous hard brittle ceramic material. Some advantages to using LSSN are: it is relatively chemically inert, non-toxic, mechanically stable, forms a hermetic seal, and has a relatively low residual stress for a thin film. Work has been done to characterize the residual stress of LSSN films with respect to deposition parameters [6] [2] [23]. Stoichiometric silicon nitride can be made using the chemical reaction found in equation 1-2. It was been found that the stress in silicon nitride changes as a ratio of $SiCl_2H_2/NH_3$ input gas flow changes. The change in the gas flow ratio causes the film to become silicon rich.

$$4NH_{3\,(g)} + 3SiCl_2H_{2\,(g)} \rightarrow Si_3N_{4\,(s)} + 6HCl_{\,(g)} + 6H_{2\,(g)} \qquad (1\text{-}2)$$

In general the film was found to have a high tensile stress when the ratio of the input gases was close to 1(or close to stoichiometric silicon nitride). The tensile stress decreased and even became compressive as the ratio of input gases was increased (or the film has higher percent silicon). In one study the range of the residual stress was found to be roughly 500 MPa to -60 MPa when changing the input gas flow ratio from 1 to 8 [2].

Some disadvantages of LSSN are: it is optically transparent for the thickness needed for good X-ray transmission which can interfere with soft X-ray measurements. It also, has a high Z number compared to beryllium. This requires a much thinner membrane for comparable X-ray transmission performance compared to beryllium.

1.7 Low Stress Silicon Nitride X-ray Window Fabrication

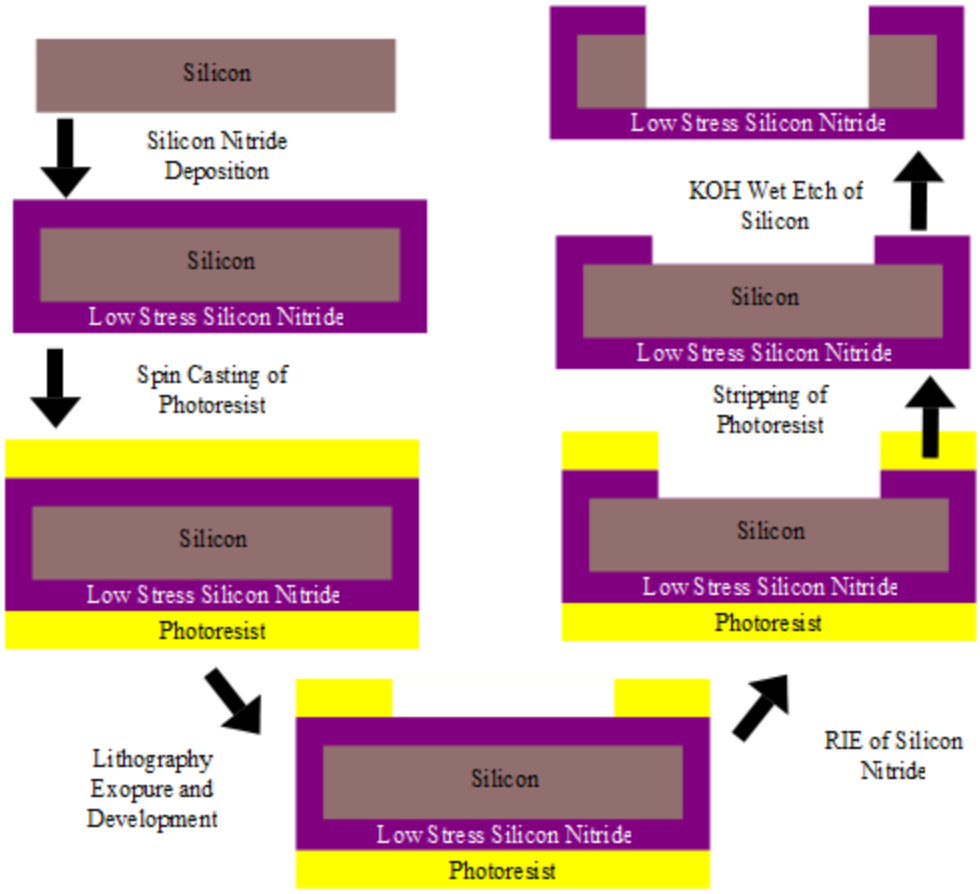

Figure 1-3 Process diagram for the low stress silicon nitride X-ray window fabrication

LSSN X-ray windows were fabricated using the general process outline in figure 1-3. LSSN was deposited on silicon wafers and then patterned using photolithography. The LSSN

exposed by the photolithography patterned was removed using reactive ion etching. The photoresists was stripped, and the exposed silicon was then removed using a KOH wet etch.

1.8 Beryllium as an X-ray Window Material

Beryllium is a brittle alkaline metal that has a steel gray appearance, and can crack easily at room temperature [22]. It will form a thin oxidation layer under ambient conditions, and readily forms alloys with other elements such as iron, nickel, aluminum, copper, and silicon at high temperatures [21]. Sputtered beryllium thin films are known to have inhomogeneous residual stress due to their columnar structure, but have been shown to withstand a pressure differential of over 1 atm [22].

Some advantages to using beryllium as an X-ray window material are: it has a low Z number allowing for good X-ray transmission, it is optically opaque, and is mechanically stable. Some disadvantages to beryllium are: beryllium dust is toxic and can cause Acute Beryllium Disease and Chronic Beryllium Disease (also known as Berylliosis) if inhaled [18] [20]. As a result, precautions must be taken to limit potential exposure. It also does not form a hermetic seal at thicknesses used for X-ray transmission.

Beryllium foil can be purchased commercially in a variety of thicknesses and can be hole punched into a variety of geometries. To limit the potential exposure to beryllium dust many beryllium thin films used in X-ray windows are purchased with a specified thickness and geometry. The beryllium thin films are then welded or brazed into window holders. The 8 micron thick beryllium X-ray windows used in this study were obtained from Moxtek Inc.

1.9 Mechanical Shock Resistance Testing

In this study a pendulum apparatus will be used to investigate both LSSN and beryllium X-ray windows to compare their resistance to mechanical shock. The pendulum arm design was

chosen to allow for both repeatability and controlled variability in the magnitude of the mechanical shocks. Mechanical shocks with a comparable magnitude could be created by releasing the pendulum arm from the same angle, and shocks of different magnitudes could be created by releasing the pendulum arm from different angles.

1.10 Study Objective

Bulge testing, burst testing, and stress characterization of low stress silicon nitride films has been done previously [34] [35], but the combination of these analyses with mechanical shock resistance has not been done. In this study the Young's modulus, residual stress, and tensile strength of LSSN are characterized. The mechanical shock resistance of LSSN with and without a silicon support structure and freestanding beryllium are measured using a pendulum shock apparatus. The burst pressure, cycling capability, and leak rates of LSSN films on a silicon support structure are measured. The material properties and performance are quantified in order to evaluate LSSN's potential as a replacement material for beryllium in X-ray windows.

Chapter 2

Fabrication of Low Stress Silicon Nitride X-ray Windows

2.1 Overview of Fabrication Process

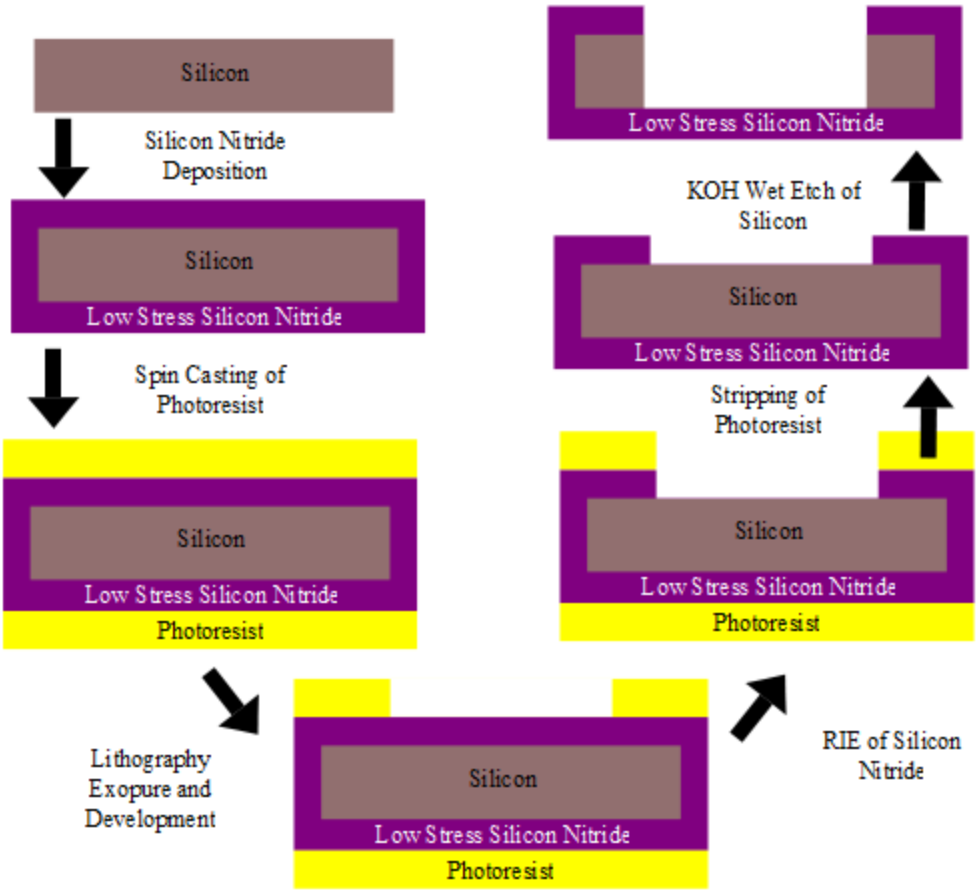

Figure 2-1 Process diagram for the low stress silicon nitride X-ray window fabrication

LSSN X-ray windows were fabricated using the general process outline in figure 2-1. LSSN was deposited on silicon wafers and then patterned using photolithography. The LSSN exposed by the photolithography patterned was removed using reactive ion etching. The

photoresist was stripped, and the exposed silicon was then removed using a KOH wet etch. Experimental details, process characterization, and fabrication results are discussed in this chapter.

2.2 Low Pressure Chemical Vapor Deposition

LSSN can be deposited on a silicon wafer using Chemical Vapor Deposition (CVD). CVD is a thin film deposition process that uses chemically reactive volatile precursors and heterogeneous nucleation to deposit thin films on a substrate. The CVD reaction depositing stoichiometric silicon nitride on a silicon wafer can be found in equation 2-1.

$$4NH_{3\,(g)} + 3SiCl_2H_{2\,(g)} \rightarrow Si_3N_{4\,(s)} + 6HCl_{\,(g)} + 6H_{2\,(g)} \qquad (2\text{-}1)$$

There are many different types of CVD systems. Some examples are thermal, atmospheric, organometallic, low-pressure, and plasma-enhanced. Stoichiometric silicon nitride is commonly deposited by either plasma-enhanced chemical vapor deposition (PECVD) or low-press chemical vapor deposition (LPCVD). LSSN, also known as silicon-rich silicon nitride, is only deposited by LPCVD and has a lower residual stress than stoichiometric silicon nitride and therefore can be subjected to higher pressures before failing as will be shown later in section 5.1.

LPCVD reactors operate at pressures below one atmosphere. A common operating pressure range is 1 to 10 mTorr [7]. Because diffusivity of the precursor gas and pressure have an inverse relationship, LPCVD reactors have the ability to deposit thin films with good thickness uniformity on many wafers at one time. Good uniformity occurs when the rate-limiting mechanism for the deposition is the kinetics of the chemical reaction, and not the availability of the precursor at the substrate surface [8].

2.3 Low Stress Silicon Nitride Deposition

Figure 2-2 Canary furnance used for LPCVD of low stress silicon nitride

The LSSN deposition was performed in a low-pressure chemical vapor deposition (LPCVD) Canary Furnace. Four inch {100} 500 micron thick double polished silicon wafers were used as a substrate for the deposition. The LSSN was deposited at a pressure of 345 mTorr and at a temperature of 825^{o} C. The flow rates for NH_3 and $SiCl_2H_2$ were 10 sccm and 60 sccm respectively. Two different target thicknesses were selected based on computed X-ray

transmission curves (section 1.4). Two wafers had a target thickness of 400±10 nm and corresponding deposition time was 63 minutes. The deposition time for the remaining two wafers with a target thickness of 600±10 nm was 99 minutes.

LSSN was also deposited on five {110} 3 inch wafers with target thickness of 100 nm for three wafers and 200 nm for the remaining two.

The thickness of the LSSN deposited on the wafers was characterized using a Nanospec 3000 reflectometer (Nanospec Pty. Lt.). The thickness of the film was measured at five locations on the wafer as indicated in figure 2-3.

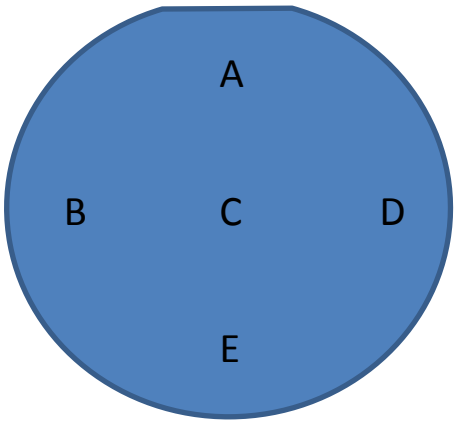

Figure 2-3 Low stress silicon nitride thickness measurement locations

The thicknesses of LSSN films deposited on the silicon substrates can be found on tables 2-1 and 2-2. The target thickness for wafers 1 and 2 on table 2-1 was 400 nm and the target thickness for wafers 3 and 4 on table 2-1 was 600 nm. The target thickness for wafers 1 through 3 on table 2-2 was 200 nm and the target thickness for wafers 4 and 5 on table 2-2 was 100 nm. The measurement locations correspond to the position the silicon wafer as shown in figure 2-3.

Wafer	A (nm)	B (nm)	C (nm)	D (nm)	E (nm)	Ave (nm)
1	410	403	405	403	390	402±7
2	406	399	401	398	388	398±7
3	648	636	636	638	619	635±10
4	639	631	630	627	613	628±9

Table 2-1 Thickness measurements of low stress silicon nitride deposited on {100} silicon wafers

Wafer	A (nm)	B (nm)	C (nm)	D (nm)	E (nm)	Ave (nm)
1	205	199	200	199	189	198±6
2	207	200	201	201	191	200±6
3	204	199	199	199	191	199±5
4	116	115	114	113	109	113±3
5	118	113	113	114	108	113±4

Table 2-2 Thickness measurements of low stress silicon nitride deposited on {110} silcon wafers

2.4 Photolithography

Once LSSN has been deposited on a silicon wafer, it can be patterned using photolithography. Photolithography is a method used to transfer a two-dimensional pattern onto a substrate. When using photolithography, substrates are first spin coated with photoresist. Photoresists are polymer compounds that are sensitive to particular wavelengths of light. When exposed to certain wavelengths the light causes a photochemical reaction which changes the crosslinking in the polymers. This in turn changes the solubility of the exposed area [9]. With a positive (or positive tone) photoresist, the photochemical reaction causes the polymer chains to be broken or disconnected. The smaller polymer chains are more soluble and are removed by

dissolving into a solvent. The removal process is called development. Positive photoresists remove the exposed area during development. With a negative (or negative tone) photoresist the photochemical reaction causes the polymers to crosslink leaving the unexposed area relatively more soluble than the exposed area. As a result, the unexposed area is removed during development.

The substrate is typically placed on a hot plate for a period of time after the photoresist is spin coated on it. This step is referred to as a soft-bake. It is used to remove solvents and stress in the photoresist and to improve adhesion to the substrate [10]. The substrate is then placed in a photolithography aligner where a patterned mask is placed between the substrate and the light source. The masks are typically made of quartz glass because it is transparent at the wavelengths that cause the photochemical reaction to occur. A metal (typically chromium or chromium and gold) is deposited in a pattern on the quartz glass. The metal absorbs the light in the patterned locations and a shadow can be found on the photoresist during exposure. The substrate is then developed in a solvent leaving behind patterned photoresist. The patterned substrate is then placed on a hot plate again for a period of time. This step is referred to as a post-bake and is used to remove the remaining solvent from the photoresist and anneal it. The photoresist can then be used as a patterned etch mask during the etching of LSSN.

2.5 Photolithography for X-ray Window Support Structure Patterning

Photoresist was used as an etch mask during the reactive ion etch process. Photoresist AZ 3312 (AZ Electronic Materials) was spin cast on both sides of the LSSN coated wafers. The wafers were then soft-baked at 90^{o} C for 1 minute. The optical photolithography exposure used a MA 150 CC Mask Aligner (Karl Suss) with a 350 W mercury blub for 4 seconds. The exposure was only preformed on one side of the wafers as shown in figure 2-1. The photoresist was

developed in AZ300 (AZ Electronic Materials) for 45 seconds. The developed wafers had one side completely covered with photoresist while the other side had patterned sections of LSSN exposed.

2.6 Reactive Ion Etching

A common method to remove LSSN is reactive ion etching (RIE) using oxygen (O_2) and tetraflouromethane (CF_4) as working gases. RIE is an anisotropic dry etch process that uses a plasma to create chemical reactive ions species that can react with the substrate to form volatile compounds which can then be removed from the system using a vacuum. It has been shown that the addition of less than 16% O_2 gas increases the etch rate due to the increased reactivity of CF_4 ions generated in the plasma [11].

The CF_4 ions do not react as readily with the photoresist. As a result, the etch rate is much slower and the photoresist acts as an etch mask. The exposed LSSN is then etched and the LSSN protected by the patterned photoresist remains. The photoresist can then be stripped by dissolving it in a solution leaving behind patterned exposed silicon.

2.7 Reactive Ion Etching of Low Stress Silicon Nitride

The exposed LSSN was etched away using reactive ion etching (RIE) which was carried out on an Anelva RIE DEM-451 (Anelva Corp.). The pressure used during the reactive ion etch was 100 mTorr and the power was 100 W. The flow rates of the O_2 and CF_4 were 3.1 sccm and 25 sccm respectively.

Figure 2-4 Anelva RIE DEM-451 used for Reactive Ion Etching

The etch rate for the LSSN and the photoresists were characterized by using 4 pieces of silicon with known thicknesses of both LSSN and photoresist deposited on them. Each one of the 4 pieces was etched for a different length of time. The etch times selected were 2, 4, 6, and 8 minutes and the thicknesses of both the LSSN and the photoresist were measured again after etching. The difference in thickness as a function of etch time were recorded. All thickness measurements were done using a M2000 spectroscopic ellipsometer (J. A. Woollam Co). The etch rate data for LSSN and Photoresist HPR 504 using RIE can be found in figures 2-5 and 2-6. The etch rates were roughly 50 nm per minute and 55 nm per minute respectively.

When fabricating the LSSN X-ray windows, the etch times were selected using the characterized etch rates. The silicon nitride wafers with target thicknesses of 400 nm and 600 nm were etched for 8 minutes 15 seconds and 13 minutes respectively, which completely removed the LSSN from the patterned locations. The remaining photoresist was dissolved off using acetone leaving behind patterned exposed silicon on one side of the wafer.

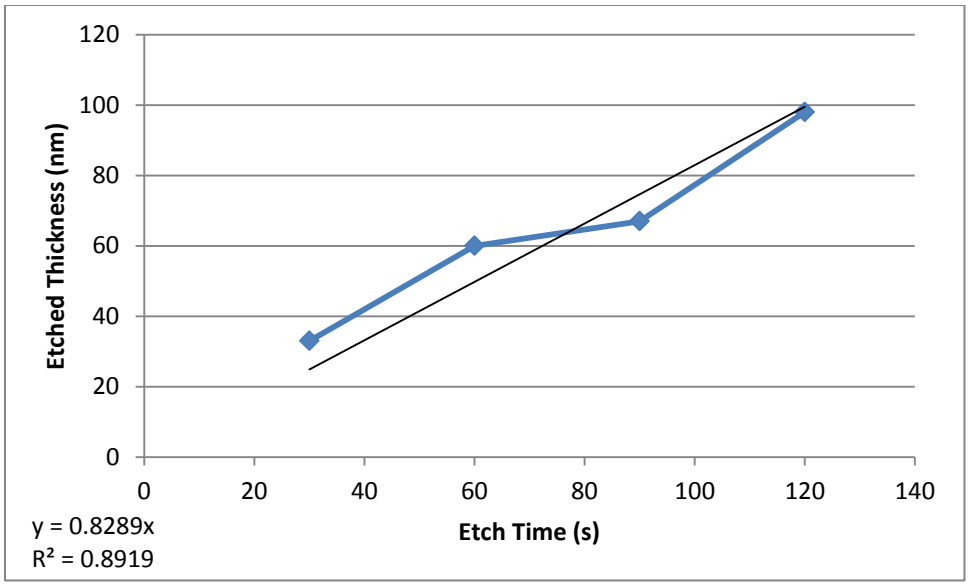

Figure 2-5 Etch rate characterization of low stress silicon nitride using RIE process

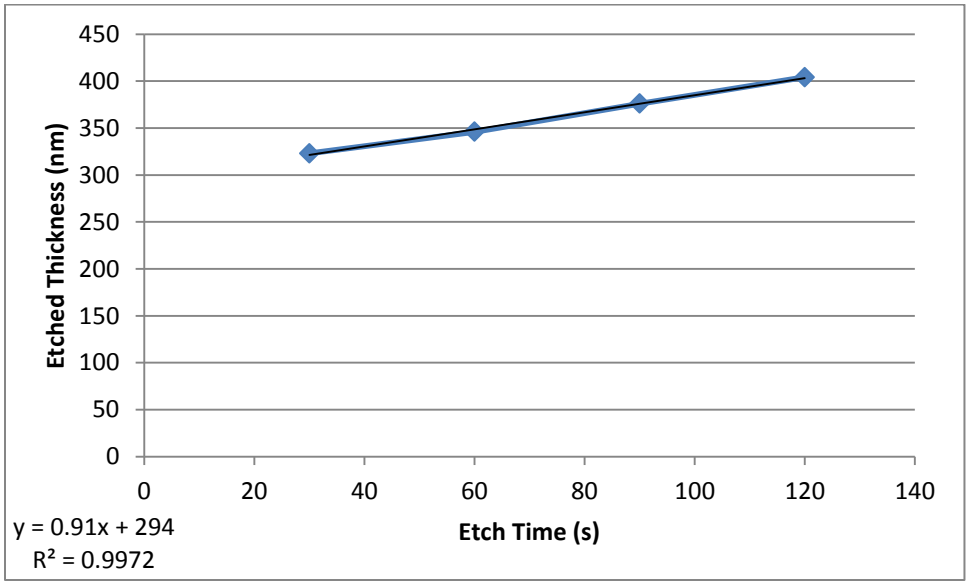

Figure 2-6 Etch rate characterization of photoresis HPR 504 using RIE process

2.8 Anisotropic KOH Etching of Silicon

Alkaline hydroxides can be used to anisotropically etch crystalline silicon. The etching chemical reaction can be found in equation 2-2.

$$2OH^-_{(aq)} + Si_{(s)} + 2H_2O_{(aq)} \rightarrow 2H_{2(g)} + SiO_2(OH)^{2-}_{(aq)} \qquad (2\text{-}2)$$

The most common alkaline hydroxide used in this type of etching reaction is KOH. The etching occurs anisotropically because the etch rates of the different crystalline planes of silicon are different. The <111> plane has the slowest etch rate compared to the <100> and the <110> planes. The etch rate ratio for <100>/<111> planes is 400 while the etch rate ratio for <110>/<111> planes is 600 when using 44 g of KOH per 100 mL of water at 80^o C [12].

Because of the anisotropic nature of the KOH etch, silicon wafers with different crystalline orientations give different geometric structures. When etching a {100} silicon wafer the <111> plane is found at 54.74^o with respect to the <100> plane on the surface of the wafer. As a result vertical trenches cannot be etched in a {100)} wafer when using an anisotropic etch. If the patterned silicon wafer was infinitely thick, a KOH etch would remove a rectangular pyramid with a slope of 54.74^o on all four sides. When using a {110} silicon wafer the <111> plane is found at 90^o with reference to the <110> plane on the surface, and as a result vertical trenches can be etched in a {110} wafer using an anisotropic etch.

LSSN doesn't react with KOH and is therefore used as both an etch mask and an etch stop for this process. The KOH can be used to etch completely through the patterned silicon leaving behind a freestanding film of LSSN on the bottom side of the wafer.

2.9 Anisotropic KOH Etching of Silicon Nitride Coated Silicon Wafers

The exposed silicon was etched in 45% concentrated KOH at 80^o C. The etch rate was characterized with 4 pieces of silicon. The thicknesses of silicon pieces were measured both before and after etching using a micrometer. The 4 silicon pieces were etched for different lengths of time. The selected time lengths were 2, 4, 6, and 8 minutes. The change in thickness

was plotted vs. etch time as shown in figure 2-7. The etch rate for the silicon in the KOH wet etch was found to be roughly 20 microns per minute.

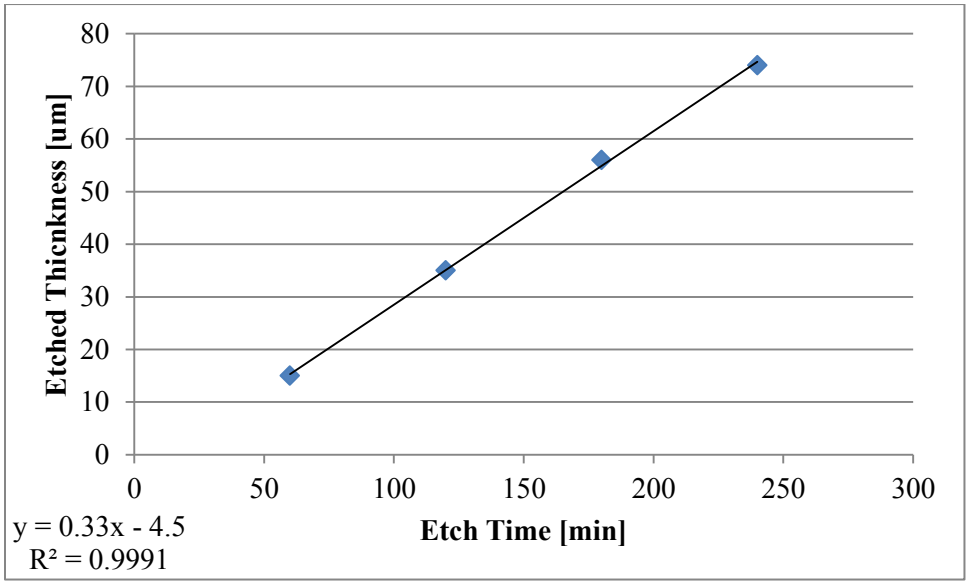

Figure 2-7 Etch rate characterization of silicon in 45% KOH at 80° C

The LSSN coated wafers were etched for 48 hours. After the KOH completely etched away the silicon in the patterned locations, only a freestanding silicon nitride membrane on the back side of the wafers remained.

2.10 Transfer of Freestanding X-ray Window Thin-Films

Aluminum washers with an outer diameter of 9 mm and an inner diameter of 7 mm were epoxied onto the freestanding LSSN thin films while they were still attached to the silicon wafer. The washers with the attached film were removed from the supporting silicon wafer, and were then epoxied into X-ray window mounts provide by Moxtek. Only 5 of the 600 nm films were transferred successfully and all of the 400 nm films were destroyed when attempting to transfer them from the support silicon wafer to the aluminum washers.

2.11 Silicon Support Structure Low Stress Silicon Nitride X-ray Window Fabrication

The silicon support structure was created by silicon ribs with a nominal thickness and spacing of 60 microns 191 microns respectively. The fabrication procedures used to make the LSSN X-ray windows on a silicon support structure were the exact same as the procedures mentioned above expect for the following deviations.

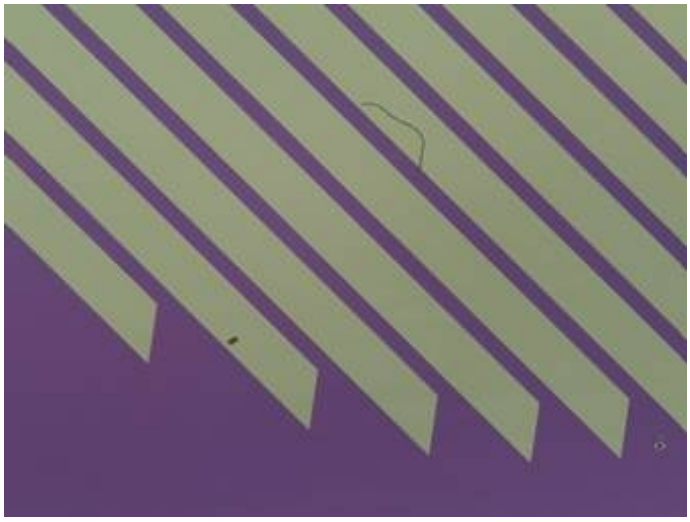

Figure 2-8 Low Stress Silicon Nitride Window on Silicon Support Structure Geometry

Silicon wafers with a {110} crystal orientation were used as a substrate for LSSN deposition to create vertically etched trenches during the KOH etch. The target LSSN deposition thickness for 2 wafers was 100 nm and the target thickness for the remaining 3 wafers was 200 nm. The LSSN deposition times were 16 and 30 minutes respectively. The thickness of the LSSN was decreased compared to the freestanding LSSN windows to compensate for the decrease in X-ray transmission caused by the presence of the silicon support structure (section 1.4). The negative photoresist used was HPR 504, and the wafers were soft-baked for 30 minutes

at 150^{o} C. The lithography was done using a Perkin Elmer aligner. The development was done in a 0.3% diluted KOH solution for 1 minute. The wafers were then hard-baked for 30 minutes at 150^{o} C. After the RIE step, the remaining photoresist was removed by soaking the wafers in Nanostrip for 4 hours. Washers were not required to remove the LSSN from the supporting silicon wafer. The thin films on the silicon support structure were removed from the silicon wafer, and epoxied onto X-ray window mounts.

Chapter 3

Low Stress Silicon Nitride Thin-Film Characterization

In this chapter the Young's modulus, residual stress, and tensile strength of LPCVD deposited LSSN films are characterized using bulge testing and curvature measurements. The experimental data and sources of error are outline in the sections below.

3.1 Thin Film Characterization

Thin film characterization techniques are require to understand the mechanical properties such as residual stress and Young's modulus of the thin film materials that can potentially be used to make X-ray windows. These thin films used for X-ray windows must be impermeable to gas and must be able to handle the stress required to maintain a pressure differential of one atmosphere on either side. The residual stress of thin films is an important property to quantify to understand a thin film's ability to handle applied stress.

3.2 Thin-film Residual Stress and Pressure

The maximum pressure that a freestanding circular thin film can withstand with fixed positions at the edges before fracturing has been modeled previously. The model assumes that the deflection is small compared to the radius of the circular opening ($r>>d$), but large compared to the thickness of the membrane so that bending at the edges can be neglected ($d>>H$). When these assumptions are made equation 3-1 can be derived [2] [25] [26] [38] [39]. The derivation of equation 3-1 can be found in Appendix A.

$$P_{max} = \frac{4H d_{max} \sigma_T}{r^2} \tag{3-1}$$

In equation 3-1, P_{max} is the maximum pressure the thin film can withstand, d_{max} is the maximum deflection of the center of the film in the normal direction, r is the radius of the window, H is the thickness of the membrane, and σ_T is the tensile strength of the material. The relationship between the tensile strength of the material and the applied stress, σ_A, caused by pressure can found in equation 3-2.

$$\sigma_T = \sigma_A + \sigma_R \tag{3-2}$$

σ_R is residual stress (with tensile stress being positive and compressive stress being negative).

According to equations 3-1 and 3-2, in order to increase the maximum pressure that a thin film can withstand with a given material and geometry, either the thickness of the film must be increased, H, or the residual stress, σ_R, must be reduced. In our application increasing the thickness would cause a decrease in X-ray transmission as shown in equation 1-1. As a result a film with a low residual stress compared to the applied stress or a film with compressive residual stress is desired.

Characterization of residual stress, Young's modulus and tensile strength of the deposited LSSN film were performed using the processes and procedures outlined below.

3.3 Bulge Testing

One method that can be used to measure the residual stress, Young's modulus and tensile strength of a material is bulge testing. A mathematical relationship between tensile strength and pressure can be found by solving equation 3-1 for σ_T.

$$\sigma_T = \frac{P_{max} r^2}{4 H d_{max}} \tag{3-3}$$

The tensile strength of a material can be found by measuring the maximum deflection at the maximum pressure.

If once again spherical geometry is assumed and the deflection of the film is small compared to the radius of the circular film, equation 3-4 can be derived. The derivation of equation 3-3 can be found in Appendix D.

$$P = \frac{4Hd}{r^2}[\sigma_R + \frac{2Yd^2}{3(1-\nu)r^2}] \quad (3\text{-}4)$$

In equations 3-3 and 3-4 P is the pressure; H, d, and r are the thickness, deflection, and radius of the membrane. In equation 3-4 Y and ν are the Young's modulus and Poisson's ratio and σ_R is the residual stress in the membrane. If, H, r and ν are known, equation 3-4 can be rewritten as equation 3-5.

$$P = \alpha d + \beta d^3 \quad (3\text{-}5)$$

Where α and β are defined in equations 3-6 and 3-7.

$$\alpha = \frac{4H\sigma_R}{r^2} \quad (3\text{-}6)$$

$$\beta = \frac{8HY}{3(1-\nu)r^4} \quad (3\text{-}7)$$

The residual stress and Young's modulus can be solved for by measuring the deflection as a function of pressure and empirically finding values for α and β that fit the data.

3.4 Bulge Testing Procedure

Because of safety concerns with beryllium dust and the complicated geometry of the silicon support LSSN X-ray windows, only the freestanding LSSN X-ray windows were used for bulge testing. Glass slides with known thicknesses were used to calibrate optical focus as a function of displacement (see figure 3-1).

The window was mounted on to the bulge testing apparatus, and the differential pressure was incrementally increased starting from 0 Pa using a flow rate valve. The deflection of the center of the membrane in the normal direction was measured at each pressure step using an

optical microscope. The pressure and deflection were recorded and the process was repeated at the next pressure step.

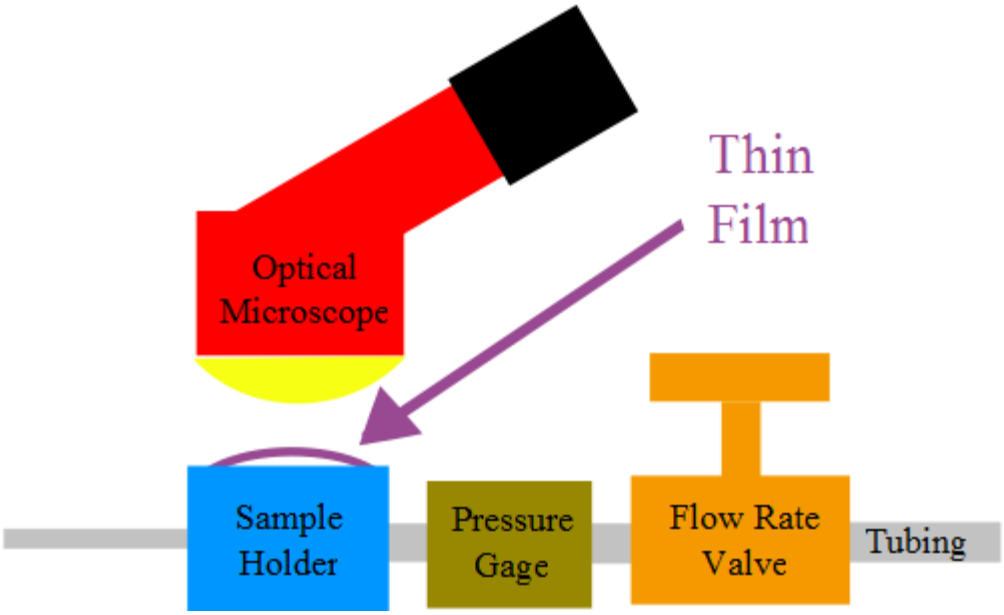

Figure 3-1 Bulge testing experimential setup. An optical microscope was used to measure the deflection of the thin film in the normal direction. A pressure gauge was used to measure the pressure and the pressure was controlled using a flow rate valve.

The deflection as a function of pressure for each of the three samples was plotted. The constants α and β in equation 3-5 were then calculated to fit the experimental data.

$$P = \alpha d + \beta d^3 \tag{3-5}$$

The constants α and β were then used to determine residual stress and Young's modulus using the measured values of $H = 6.39 \times 10^{-9}$ m and $r = 3.5 \times 10^{-3}$ m. A value of 0.25 was used for the Poisson's ratio for LSSN [28]. These values were substituted into equations 3-6 and 3-7 to solve for residual stress and Young's modulus respectively.

$$\alpha = \frac{4H\sigma_R}{r^2} \tag{3-6}$$

$$\beta = \frac{8HY}{3(1-\nu)r^4} \tag{3-7}$$

The bulge test was also used to determine the tensile strength of the material. The applied pressure that caused the thin films to rupture was recorded and the fracture displacement was determined by extrapolation using equation 3-5 and the calculated constants for each of the films. Equation 3-8 was used to calculate the tensile strength of the thin-film using the max pressure and the max displacement as well as the values for *H* and *r* mentioned above.

$$\sigma_T = \frac{P_{max}r^2}{4Hd_{max}} \tag{3-8}$$

The pressure vs. deflection data points as well as their corresponding calculated lines using equation 3-5 can be found on figure 3-2. The values found for residual stress, tensile strength, and Young's modulus for each of the films and the average of each of these quantities can be found on table 3-1. The average residual stress, tensile strength, and Young's modulus were found to be 1.41±0.28 x 10^8 Pa, 8.75±0.40 x 10^8 Pa, and 2.26±0.23 x 10^{11} Pa respectively.

Property	**Film A**	**Film B**	**Film C**	**Ave**
Residual Stress [Pa]	**1.64 x 10^8**	**1.10 x 10^8**	**1.49 x 10^8**	**1.41±0.28 x 10^8**
Tensile Strength [Pa]	**8.78 x 10^8**	**8.32 x 10^8**	**9.13 x 10^8**	**8.74±0.40 x 10^8**
Young's Modulus [Pa]	**2.11 x 10^{11}**	**2.52 x 10^{11}**	**2.15 x 10^{11}**	**2.26±0.23 x 10^{11}**

Table 3-1 Residual stress, tensile strength, and Young's modulus for three low stress silicon nitride films using bulge testing

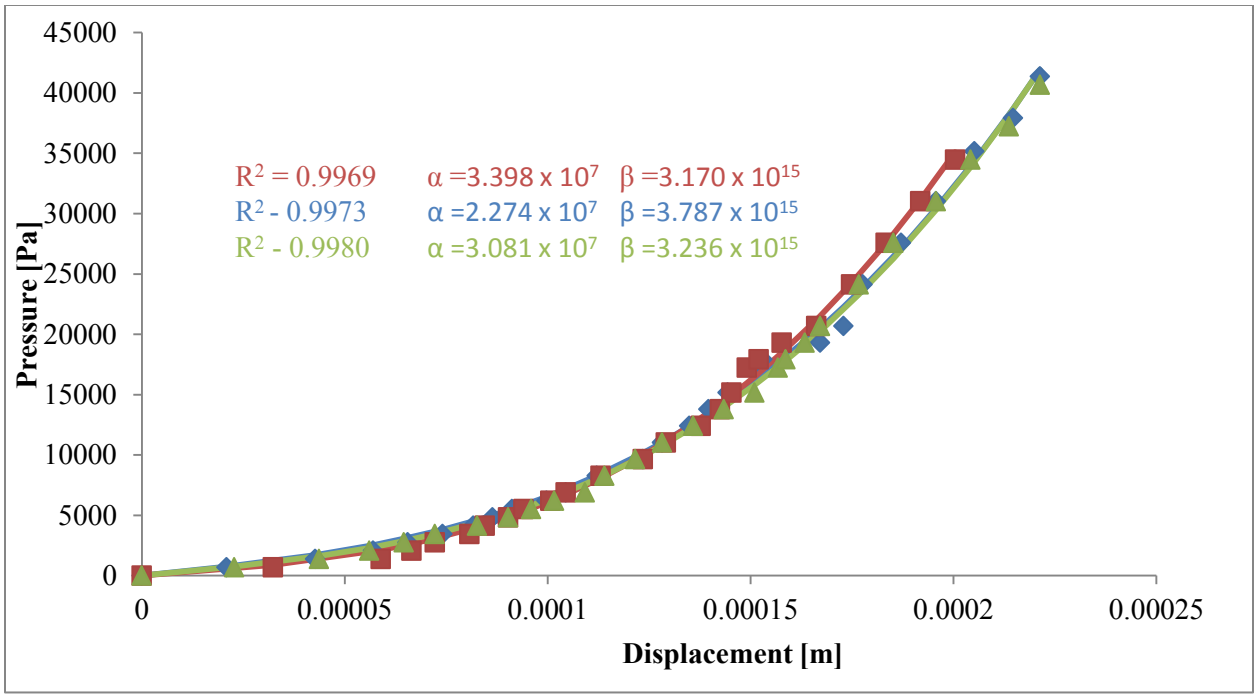

Figure 3-2 Pressure and film defection measurements and calculated lines using equation 3-5.

3.5 Sources of Error for Bulge Testing

The precise distance that brings the film into focus is difficult to measure with the naked eye, and may lead to some errors in the deflection measurements. The range of focus was roughly 20 microns. An attempt was made to record the deflection height at the center of the focus range, but the deflection height measurements could be off by as much as 5 microns. An error of 5 microns in the deflection height will change the calculated Young's modulus value by $\pm 10 \times 10^{10}$ Pa, the residual stress value by $\pm 3 \times 10^{-7}$ Pa, and the tensile strength of the material by $\pm 5 \times 10^{-7}$ Pa. The R^2 values shown on figure 3-2 are relatively close to unity which provides evidence that if there are errors in the deflection height measurements, they are likely systematic.

The value for the Poisson's ratio of 0.25 for LPCVD deposited LSSN was found in the literature and not directly measured [28] [29]. The actual value may vary from 0.23-0.27. The variation can change the value of the calculated Young's modulus by $\pm 2 \times 10^{10}$ Pa.

3.6 Stoney Equation and Wafer Curvature

Another method that is used to characterize residual stress in a thin film is by measuring the curvature of a substrate before and after a thin film is deposited on one side. When the thickness of the deposited thin film is much smaller than the thickness of the substrate, a good approximation of the film stress can be given by equation 3-9 which is a variation of the Stoney equation [5] [36].

$$\sigma_R = \frac{Y_s {H_s}^2}{6R_{eff}(1-\nu_s)H_f} \tag{3-9}$$

In equation 3-9, Y_s is the Young's modulus of the substrate, R_{eff} is the effective radius of curvature, v_s is the Poisson's ratio of the substrate, and H_s and H_f are the substrate and film thicknesses respectively. This equation is derived by equating the bending moments of the film and substrate to the force due to the thin film and the thickness of the film and substrate.

R_{eff} can be determined by finding the curvature, κ, which is defined as the inverse of the radius of a circle or curve as shown in equation 3-10.

$$\kappa = \frac{1}{R} \tag{3-10}$$

The effective radius of curvature can be found by taking the inverse of the difference between the final and initial curvatures.

$$R_{eff} = \frac{1}{\kappa_f - \kappa_i} = \frac{R_f R_i}{R_i - R_f} \tag{3-11}$$

In the limit that the initial curvature is zero, or in other words the substrate is initially perfectly flat, the effective radius is the inverse of the final curvature and original definition of curvature found in equation 3-10 is recovered. Curvature of a function can be found by taking

the second derivative. By using a parabola to fit the curvature of the substrate we can recover the following relationships.

$$f(x) = ax^2 + bx + c \tag{3-12}$$

$$f''(x) = 2a = \kappa = \frac{1}{R} \tag{3-13}$$

$$R = \frac{1}{2a} \tag{3-14}$$

As shown in equation 3-14, the radius of curvature is equal to the inverse of two times this first coefficient of the parabolic equation [37].

3.7 Stoney Equation and Wafer Radii of Curvature Measurements

The film should be deposited on one side of the substrate in order to measure a difference in residual stress using changes in curvature. During the LPCVD deposition of LSSN, the film is coated uniformly across the entire wafer, therefore the LSSN on one side of the wafer needs to be etched away without etching away any of the silicon. Two wafers with average LSSN thicknesses of 189 nm and 92 nm had photoresist AZ 3312 (AZ Electronic Materials) spin cast on them. The RIE process was then used to etch the wafers for 3 minutes and 47 seconds and 2 minutes and 50 respectively. The etch times were determined using the etch rate characterizations done in section 2.7 figure 2-5, and an attempt was made to etch to the interface between the LSSN and the silicon substrate in order to remove as much of the LSSN as possible without over etching and removing some of the silicon wafer. After the wafers were etched there were no visual signs of LSSN one of the sides.

The radii of curvature of the two wafers were measured both before and after LSSN deposition using a Zygo Mesa interferometer. The measurement provided a contour plot of the wafer surface. Line profiles of the contour plot were fit to parabolic functions using the open

source software Gwyddion. The constant on the quadratic term was used to determine the radius of curvature as outlined in equation 3-15.

$$R = \frac{1}{2a} \tag{3-15}$$

The effective radius of curvature was determined by using radius of curvature measurements from before and after LSSN deposition and equation 3-16.

$$R_{eff} = \frac{1}{\kappa_f - \kappa_i} = \frac{R_f R_i}{R_i - R_f} \tag{3-16}$$

Four line profiles roughly the length of the wafer diameter going through the center of the silicon wafer were drawn in the same locations of the wafer both before and after the LSSN deposition. The four lines were 45^{o} apart from the adjacent lines. A picture of the line profile location can be found in figure 3-3. The line profiles went across the entire wafer, but are only drawn to the center in figure 3-3 to clearly see the directions and orientations. The residual stress was calculated for all four lines and averaged to estimate the overall residual stress in the film. The stress was then determined by using the calculated effective radius of curvature and other known parameters of the system in equation 3-17.

$$\sigma_R = \frac{Y_s {H_s}^2}{6R_{eff}(1 - \nu_s)H_f} \tag{3-17}$$

The wafer thicknesses, H_s, were measured and the average value was found to be 500 microns. The values for the Young's modulus and Poisson ratio of the silicon wafer substrate were assumed to be 1.6 x 10^{11} Pa and 0.27 respectively [41] [44] [45].

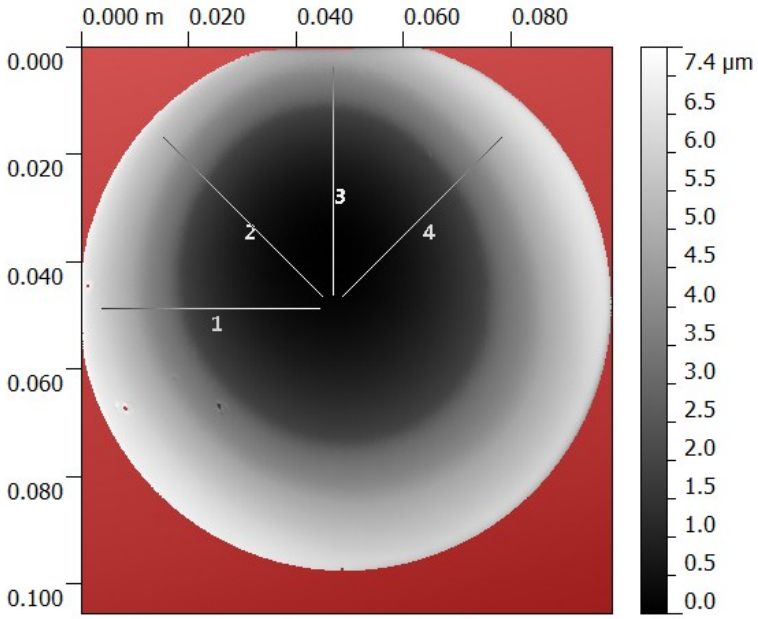

Figure 3-3 Line profile locations used to measure radii of curvature. The actual line ran across the entire wafer, but they are only partital draw on this figure for clarity

Images of the differences in curvature of a silicon wafer before and after LSSN deposition can be found in figure 3-4. The calculated residual stress for each line profile as well as the average residual stress for both films can be found on table 3-2. The average residual stress found for the film with the average thickness of 189 nm was 1.30±0.25 x 10^8 Pa, and the average residual stress found for the film with the average thickness of 92 nm was 1.24±0.60 x 10^8 Pa. The line profile location corresponds to those shown in figure 3-3.

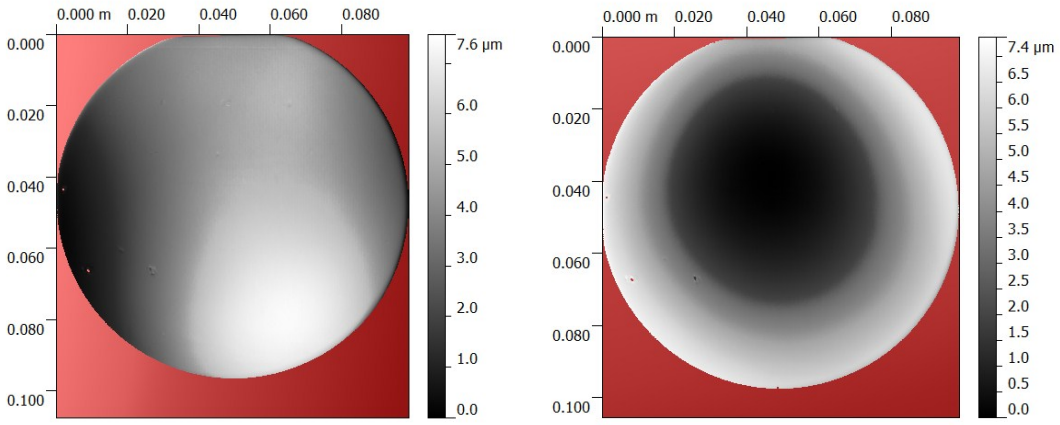

Figure 3-4 Differences in cuvature of the same wafer before and after low stress silicon nitride deposition

Location	189 nm Film	92 nm Film
1 (Pa)	1.06×10^8	1.36×10^8
2 (Pa)	1.58×10^8	2.16×10^8
3 (Pa)	1.45×10^8	5.41×10^7
4 (Pa)	1.11×10^8	9.16×10^7
Ave (Pa)	$1.30 \pm 0.25 \times 10^8$	$1.24 \pm 0.60 \times 10^8$

Table 3-2 Residual stress measurements for etch line profile and the average.

3.8 Sources of Error for Wafer Radii of Curvature Measurements

The values for the Young's modulus and Poisson's ratio of the silicon substrate found in the literature were used and not directly measured. The values were 1.6×10^{11} and 0.27 respectively [41]. Silicon is a very well-studied material, and the actual values of Young's modulus and Poisson's ratio vary depending on crystal orientation and sample. The ranges found

in the literature at $1.33 \times 10^{11} - 1.88 \times 10^{11}$ Pa and 0.36-0.064 [41] [44] [45]. The variation in both of these properties can change the value of the residual stress by up to 30%.

In order to accurately measure the change in the radius of curvature of a silicon wafer substrate, the thin film should only be deposited on one side. This is easily done when using line-of-sight deposition processes such as evaporation or sputtering. In our case, LPCVD was used to deposit the LSSN on the silicon wafer substrates. LPCVD deposits the film on both sides of the wafer, and therefore one side of the LSSN needed to be etched away. The etch rate characterization of the LSSN was used to determine etch times that in theory would remove all of the LSSN on one side of the wafers without removing any of the silicon on the substrate. In practice it is unlikely that the etch process was stopped right at the interface between the substrate and the LSSN. There is some non-uniformity in the RIE rate over at different locations on the wafer and the etch rate can vary from run to run. As a result, the change in the radii of curvature of the wafers was most likely not due solely to the thin film deposition on one side. If the film was over etched the curvature of the initial silicon substrate would change. If the film was under etched the effective radius of curvature would decrease because of the film on the opposite side causing the wafer to curve slightly in the opposite direction. The standard deviation for etch rates for the LSSN is 10 nm per minute, therefore the etch may have stopped 20 nm away from the interface for the sample with a LSSN thickness of 189 nm and 10 nm away from the interface for the sample with the 92 nm thick LSSN. The change of thickness of 10 nm will change the residual stress by $\pm 3 \times 10^{7}$ Pa.

3.9 Characterization Results and Literature Comparison

The value for the Young's modulus found using the bulge test for the LSSN was found to be 226±23 GPa. Young's modulus values reported in the literature for LPCVD deposited LSSN varies from 373 GPa to 186 GPa [27]. The value found in this experiment is consistent with those found in the literature.

The value for the residual stress found using the bulge equation was 141±28 MPa, and the average value of the residual stress of the LSSN using the Stoney equation was 130±25 MPa. These values are in reasonable agreement with each other. Residual stress measurements reported in the literature for LPCVD deposited LSSN varies from 1.3 GPa (tensile) to -52 MPa (compressive). As mentioned in section 1.6 the ratio of the input gases during deposition can have an effect on the magnitude and sign of the residual stress. The input ratio of $SiCl_2H_2/NH_3$ used in our deposition was 6, and the residual stress found in this study is within the range reported in the literature using similar input gas ratios (125-430 MPa) [2] [27].

The tensile strength of the LSSN was found to be $8.75\pm0.40 \times 10^8$ Pa. This value is one order of magnitude lower than the values found in the literature. This difference in the values found may be attributed to edge effects caused by the epoxy used to transfer the thin films on to washers.

Also the linear analysis done in this study does not take into account nonlinear effects caused by bending at the edges. A more complete analysis that includes these nonlinear effects needs to be done [29],[46].

Chapter 4

Beryllium and Low Stress Silicon Nitride X-ray Window Testing

The X-ray windows were subjected to a series of tests to compare their potential performance. A burst test was performed to investigate when the films would fail due to stress caused by a pressure differential. Cycling and leak rate testing was done to verify reliability in applications where pressure cycling occurs regularly. A mechanical shock resistance test was done to simulate mechanical shocks that may potentially occur to hand held devices if they were dropped. Experimental procedures and results are discussed in this chapter.

4.1 Burst Testing

LSSN X-ray windows on silicon support structures of both 100 nm and 200 nm thicknesses were tested. The silicon support structure was created by silicon ribs with a nominal thickness of 60 microns and a nominal spacing 191 microns. The burst testing for beryllium windows was not performed due to safety concerns. The burst pressure for freestanding LSSN windows was obtained through bulge testing.

The burst test was performed by increasing the pressure on one side of the film at a constant rate until the film ruptured. The pressure as a function of time was recorded and the highest pressure applied before the film ruptured is reported.

Burst pressure results can be found on table 4-1. The average burst pressure for the 200 nm thick LSSN X-ray window on a silicon support structure was found to be 227 kPa and the average burst pressure for the 100 nm thick LSSN windows with the same geometry was found to be 138 kPa.

Thickness	Window 1	Window 2	Window 3	Window 4	Window 5	Average
100 nm	131 kPa	62 kPa	82 kPa	103 kPa	310 kPa	138±100 kPa
200 nm	207 kPa	303 kPa	227 kPa	269 kPa	131 kPa	227±65 kPa

Table 4-1 Burst pressure for 100 nm and 200 nm thick low stress silicon nitride X-ray windows on a silicon support structure

The average values for the burst pressures for the 100 nm and 200 nm LSSN X-ray windows on the silicon support structure were 1.4 atm and 2.2 atm respectively. Beryllium windows with a freestanding circular geometry with a 7 mm diameter can handle a pressure difference of up to 2 atm without failing according to the specification sheet provided by Moxtek Inc. The average value for the burst pressure was 0.4 atm for the 600 nm thick LSSN X-ray windows with a freestanding circular geometry and a 7 mm diameter . Although the exact burst pressure for the beryllium windows was not found, the specification sheet upper limit is greater than all of the LSSN window except for the 200 nm thick window on the silicon support structure.

There is a very large variance in burst pressure from sample to sample. When the samples would burst, both the film and the silicon support structure would rupture. Defects have a significant influence on the mechanical failure behavior of materials. In this study the defects were not characterized and as a result it is difficult to provide a mechanism as to why there is a large variance in burst pressures.

4.2 Cycling and Leak Rate Testing

Both 200 nm and 100 nm thick LSSN X-ray windows were placed on the cycling apparatus. The apparatus would apply a pressure difference of 1 atm to one side of the window and then remove it. The pressure cycling was repeated. The leak rates of the windows were

measured after the 25th, 150th, and 500th cycles. The leak rate was investigated by testing the helium permeability of windows using a Leybold Phoenix xl 300 modul leak rate tester (Oerlikon Leybold Vacuum). A window with leak rate equal to or less than 10^{-10} mbar-L/s was classified as acceptable, while a window with a leak rate greater than 10^{-10} mbar-L/s was classified as unacceptable.

Beryllium X-ray windows are regularly subjected to cycling and leak rate testing during production at Moxtek. They have been shown to have been able to display acceptable leak rates after over 100 cycles. Freestanding LSSN X-ray windows were not able to withstand a pressure differential of 1 atm and were therefore not cycled or leak-rate tested.

Leak rates at the 25th, 150th, and 500th cycles are given on table 4-2. Only 1 of the 100 nm windows had an acceptable leak rate at the 25th and 150th cycles. That same window failed by the 500th cycle. Two of the 200 nm thick windows had an acceptable leak rate at the 25th, 150th, and 500th cycles.

The manufacturing quality control specification requires that leak rate for the beryllium windows provided by Moxtek be less than 1×10^{-10} mbar-L/s and the window should maintain that leak rate specification for at least 100 cycles. Both of the 100 nm and 200 nm thick LSSN windows on the support structure had windows that met those same specifications, but the yield was very low (three of the five for both thicknesses) as shown on table 4-2.

Thickness	25 Cycles [mbar-L/s]	150 Cycles [mbar-L/s]	500 Cycles [mbar-L/s]
100 nm	2×10^{-7}	1×10^{-7}	1×10^{-7}
100 nm	5×10^{-7}	2×10^{-8}	3×10^{-7}
100 nm	1×10^{-6}	1×10^{-6}	5×10^{-7}
100 nm	Failure		
100 nm	1×10^{-12}	1×10^{-12}	Failure
200 nm	5×10^{-4}	5×10^{-4}	1×10^{-3}
200 nm	1×10^{-12}	1×10^{-12}	1×10^{-12}
200 nm	1×10^{-7}	5×10^{-8}	3×10^{-8}
200 nm	1×10^{-12}	1×10^{-12}	1×10^{-12}
200 nm	3×10^{-7}	2×10^{-6}	1×10^{-6}

Table 4-2 Leak rates at the 25th, 150th, and 500th cycles for 100 nm and 200 nm thick low stress silicon nitride X-ray Windows on a silicon support structure

4.3 Mechanical Shock Resistance Apparatus and Shock Characterization

In this study a pendulum apparatus will be used to study the mechanical shock resistance of both LSSN and beryllium, X-ray windows. The pendulum arm design was chosen to allow for both repeatability and controlled variability in the magnitude of the mechanical shocks. Mechanical shocks with a comparable magnitude could be created by releasing the pendulum arm from the same angle. Mechanical shocks of different magnitudes could be created by releasing the pendulum arm from different angles.

The apparatus consisted of a pendulum arm which could be suspended at various angles using a stainless steel pin. By removing the pin the pendulum arm was released and allowed to

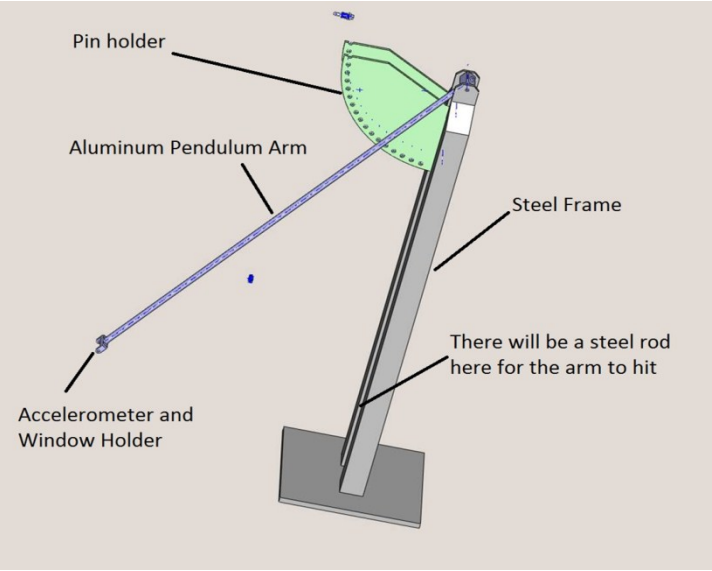

Figure 4-1 X-ray window and accelerometer holder located at the end of the pendulum arm of the mechanical shock apparatus

swing down freely to strike a stainless steel crossbar. The impact between the pendulum arm and the crossbar resulted in a mechanical shock wave which propagated to the X-ray window. The magnitude of the mechanical shock wave could be increased or decreased by varying the angle from which the pendulum arm was released.

The acceleration was measured using a 350B24 accelerometer (PCB Piezotronics).The accelerometer and the window were mounted to the end of the pendulum arm just below the contact point between the pendulum arm and the cross bar. The X-ray window mounts were tightened against a rubber O-ring by screwing on the apparatus using a mount cover. A vacuum tube connected to a roughing vacuum pump was attached to the window for two reasons. The windows used in hand held devices are under vacuum, and therefore the vacuum was used to simulate practical device conditions. The vacuum also provided a detection mechanism to look at the possible hermetic failure of the window.

The acceleration and the resulting mechanical shock wave for each release angle was recorded in order to characterize the expected mechanical shock that the X-ray would be exposed to. The acceleration vs. pendulum arm release angle data can be found in figure 4-3.

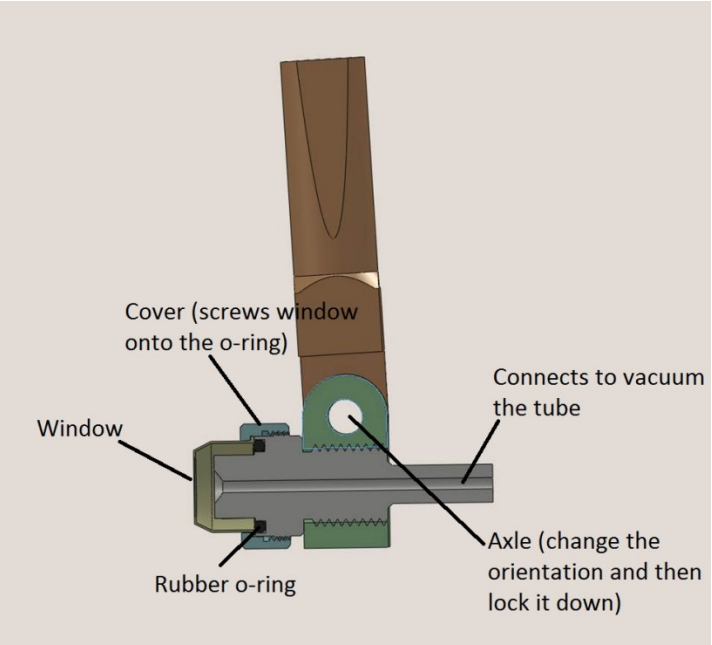

Figure 4-2 Cross section of the X-ray window holder and accelerometer at the end of the pendulum arm of the mechanical shock apparatus

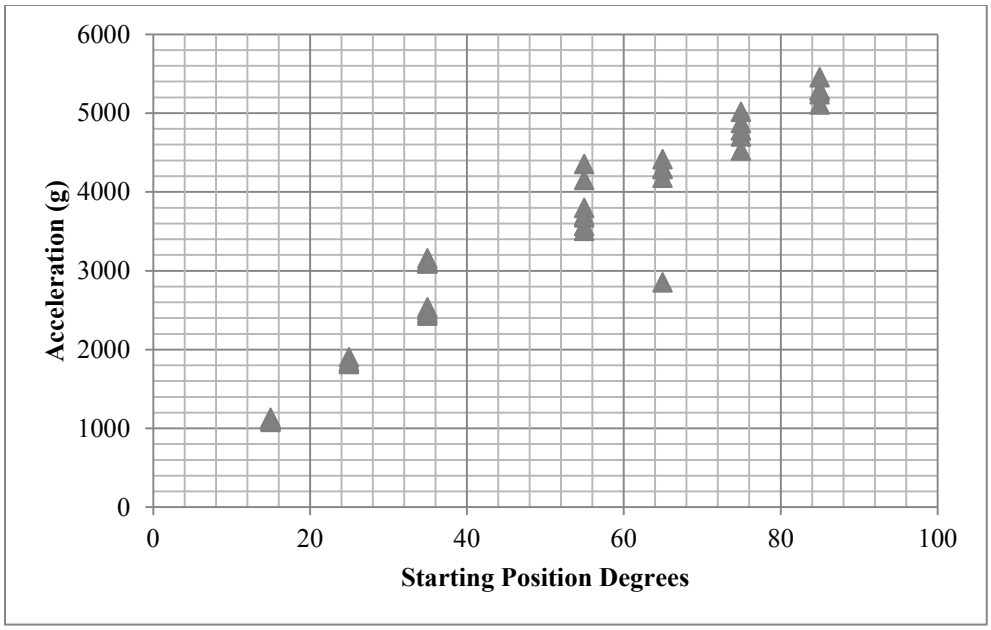

Figure 4-3 Maximum mechanical shock provided by the mechanical shock pendulum apparatus from a variety of release angles

In order to compare the magnitude of a mechanical shock that a device may be subjected to when dropped, the accelerometer was mounted to a piece of Teflon and dropped from varying heights and the acceleration was recorded. This comparison could be used to relate the release angles to drop heights. The maximum measured acceleration when dropped for a variety of heights can be found in figure 4-4 and can be used to compare release angles to drop heights. Acceleration data for the drop heights of 2.5 and 3 feet can be found on figures 4-5 and 4-6 respectively matches the maximum accelerations correspond with the data found on figure 4-4.

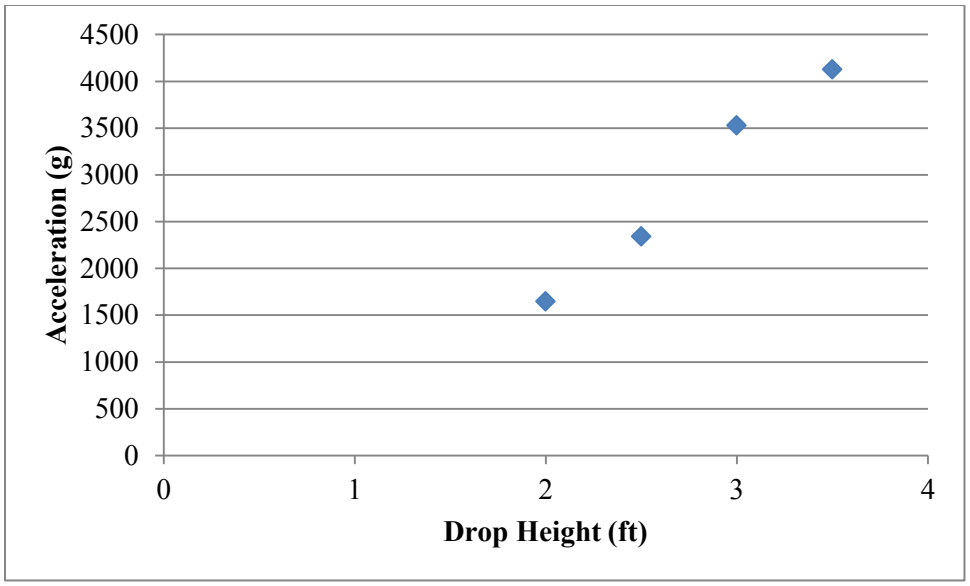

Figure 4-4 Maximum acceleration measured from droping an accelerometer from various heights

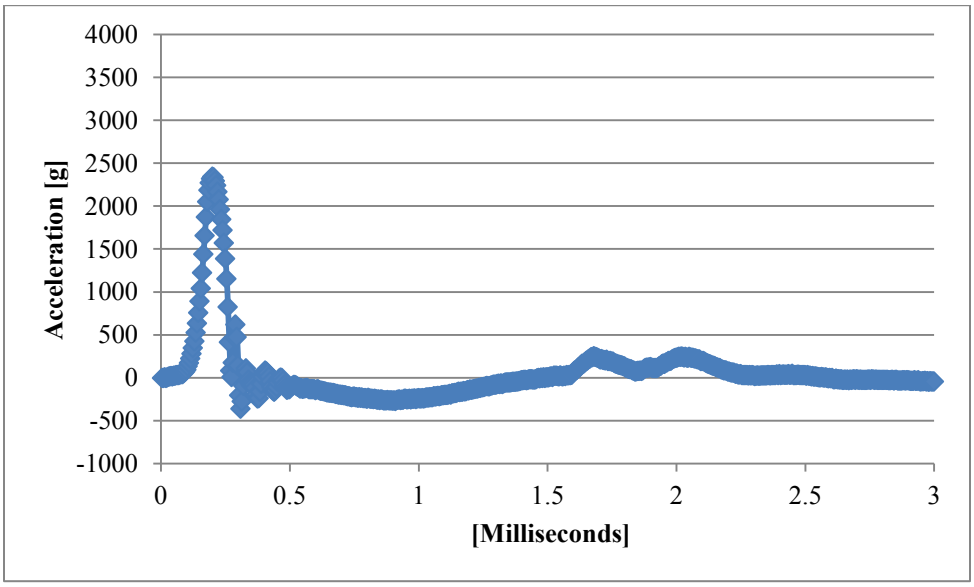

Figure 4-5 Acceleration data for an objected dropped from a height of 2.5 feet.

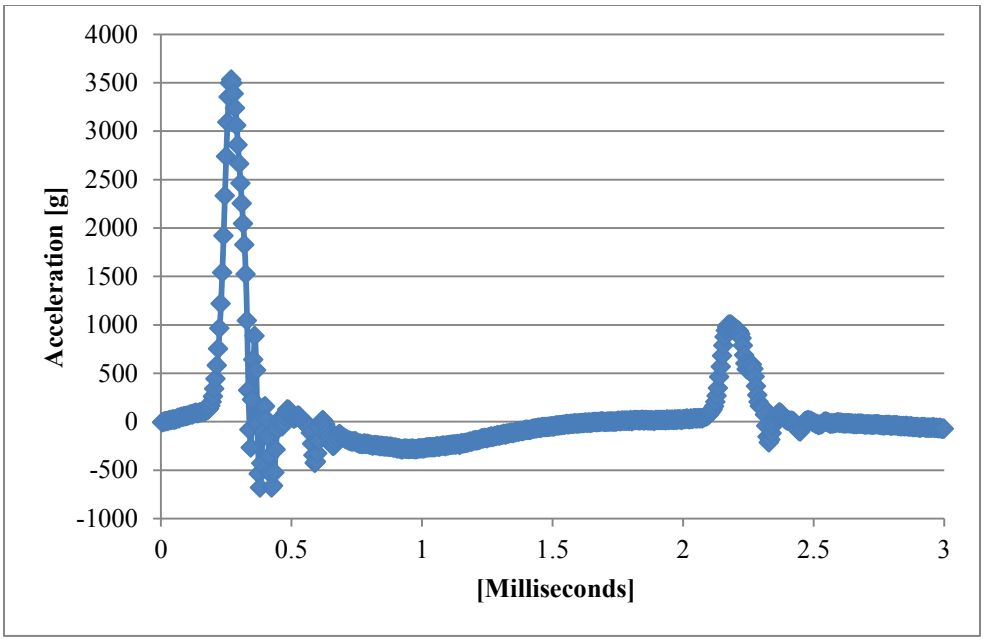

Figure 4-6 Acceleration data for an objected dropped from a height of 3 feet.

4.4 Mechanical Shock Resistance Testing

The following procedure was used to test both the beryllium and silicon support structure LSSN X-ray windows. The accelerometer and the X-ray window were attached to the shock apparatus and the pressure was pumped down to 30 mTorr or less. The pendulum arm was then released and allowed to strike the stainless steel cross bar. The acceleration of the pendulum arm was recorded using the accelerometer before, during, and after the shock. After each release, the maximum acceleration was recorded, and the vacuum pressure and the thin film window were examined to verify that the film withstood the mechanical shock without failing. The process was repeated until the maximum angle of release was reached or the window failed.

If the X-ray window was able to withstand the mechanical shock when released from an angle of 90 degrees, the pendulum arm would then be raised to an angle greater than 90 degrees and released manually. This procedure was repeated and the release angle was increased each time. If the window was able to withstand the mechanical shock when released from an angle

near 180 degrees, the pendulum was then released from an angle greater than 90 degrees and additional acceleration was manually applied to the pendulum arm to increase the magnitude of the mechanical shock. Some of the largest shock magnitudes were created by slamming the pendulum arm down with as much strength and skill as could be mustered.

The 100 nm and 200 nm thick LSSN X-ray windows with the silicon support structure and the freestanding beryllium windows were tested with an applied vacuum. The freestanding 600 nm LSSN X-ray window geometry was not able to withstand the stress required to hold a vacuum of 30 mTorr of less. As a result the mechanical shock test was performed with the same procedure outlined above without a vacuum.

Results for the mechanical shock resistance test can be found in figure 4-7. Each bar line on the figure represents the maximum acceleration recorded for a given geometry during a shock. The blue bars represent shocks where the window did not rupture, and the red bars represent shocks where the window ruptured. The 100 nm thick LSSN windows with a support structure broke with an acceleration range of 5,000 to 6,000 g. The 200 nm thick LSSN windows with a silicon support structure broke in an acceleration range of 3,300 to 5,000 g. The 8 micron thick beryllium X-ray windows were subjected to accelerations of up to 30,000 g without failure. The 600 nm thick freestanding LSSN windows that were tested without a vacuum withstood accelerations of up to 12,000 g without failure.

The freestanding beryllium and LSSN windows on the silicon support structure were able to handle the stress required to hold a vacuum and were therefore tested with a vacuum. It was found that the 100 nm silicon nitride windows were able to withstand larger shocks than the 200 nm windows made of the same material and structure. The acceleration range where the windows failed was measured for 100 nm thick silicon nitride windows with the silicon support

geometry and found to be 5,000 to 6,000 g. The acceleration shock range measured where the 200 nm film windows failure with the same geometry was found to be 3,300 to 5,000 g. 5,000 g is an acceleration that one would expect to see when dropping an object from a height between 5 to 6 ft. 3,300 g is an acceleration that one would expect to see if an objected was dropped from a height of roughly 3 ft.

The freestanding LSSN windows were not able to handle the stress caused by the difference in pressure. Therefore they were mechanical shock tested, but without an applied vacuum. The windows were subjected to accelerations of up to 12,000 g without failing. This value of acceleration is much higher than the value at which the support structure LSSN windows failed. One possible explanation for the difference in performance may be the absence of the stress by the vacuum on the silicon support structure windows. The total stress on the freestanding window will be substantially less when the stress caused by the pressure differential is removed.

Beryllium windows were found to be able to withstand shocks much greater than silicon nitride with silicon support structure geometry. There were no beryllium windows which met catastrophic failure due to shocks. Beryllium windows were able to withstand accelerations of up to 30,000 g without failing.

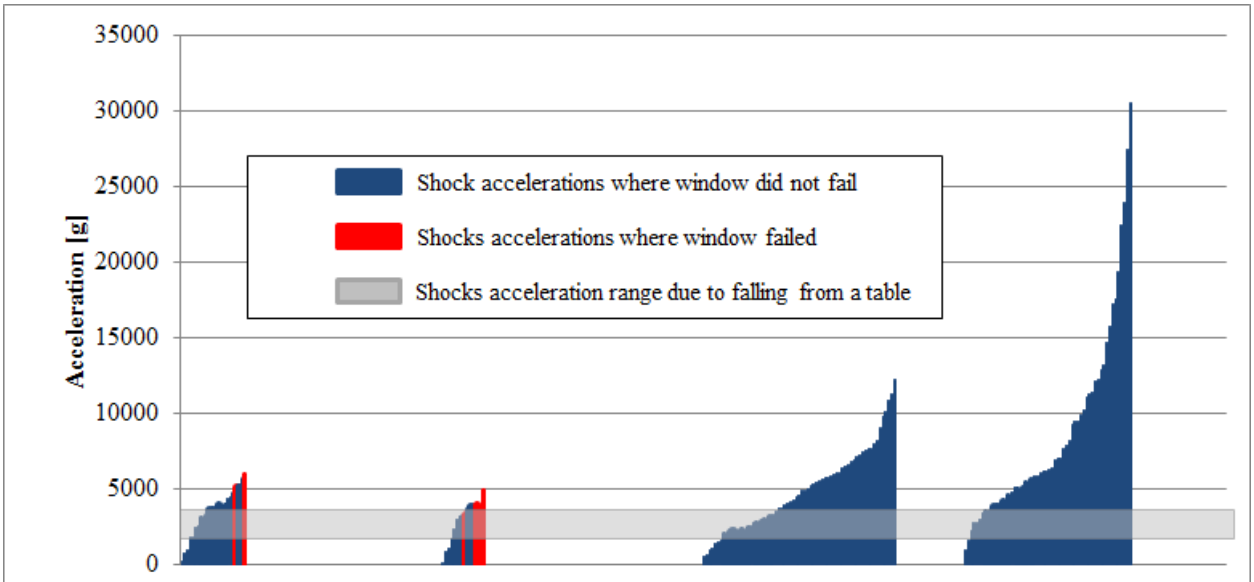

Material	Silicon Nitride	Silicon Nitride	Silicon Nitride	Beryllium
Thickness	100 nm	200 nm	600 nm	8 micron
Vacuum	Applied	Applied	Not Applied	Applied
Geometry	Silicon Ribs	Silicon Ribs	Free Standing	Free Standing

Figure 4-7Maximum acceleration measurement per mechancial shcok test. Blue bar lines represent shock accelerations where the windows did not rupture and red data points represent data points where the windows ruptured. The gray acceleartion range represents expected accelerations if an object was dropped from a desk.

4.5 Mechanical Shock Testing of AP3.3 (Brief Insights)

AP3 X-ray windows were attached to the pendulum arm while characterizing the shock caused by releasing the pendulum arm from different (See figure 4-3). The exact accelerations and pressures were not recorded while the AP3 X-ray windows were attached, but images were taken of the windows after they had been shocked. Figure 4-8 is an optical image of an AP3 window that shows cracking. The cracks were circularly symmetrical around the center of the window. It's thought that the Duracoat layer on the AP3 windows cracked during shock testing. More testing would need to be done to verify this hypothesis.

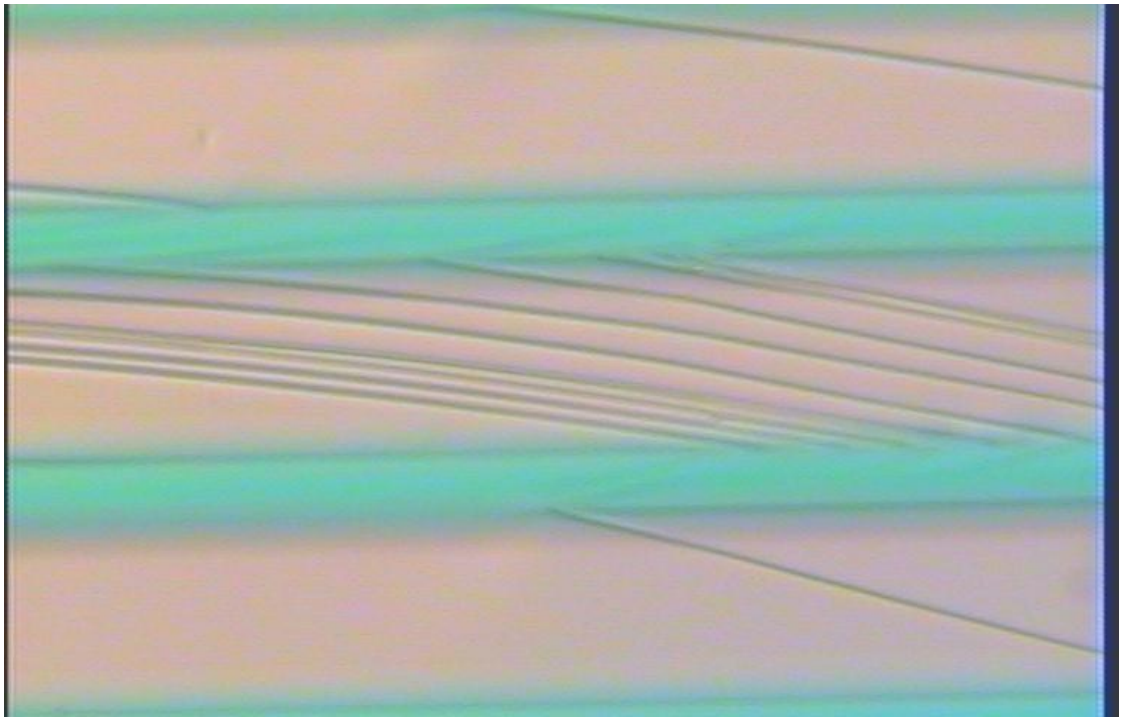

Figure 4-8 AP3 windows provided by Moxtek were attached to the shock test apperatus while characterizing the shock from various release angles. The cracks shown in the image are have circular symmetry around the center of the window. The crack are possibly in the Duracoat layer.

Chapter 5

Analysis and Discussion

5.1 Pressure and Stress on Thin Films

A few assumptions were made in order to model the applied stress on a thin-film due to pressure. The model assumes the thin film is circular, that the membrane has spherical geometry when deflected due to pressure, the deflection of the thin film is small compared to the radius of the film, and that bending at the film radius can be ignored because the thickness of the film is small compared to the deflection. When these assumptions are made, equation 5-1 can be derived. The derivation of equation 5-1 and 5-2 can be found in Appendices A and D respectively.

$$\sigma = \frac{Pr^2}{4Hd} \tag{5-1}$$

$$P = \frac{8HYd^3}{3(1-\nu)r^4} + \frac{4H\sigma_R d}{r^2} \tag{5-2}$$

By substituting equation 5-1 and in for *d* into equation 5-2 equation 5-3 can be derived.

$$P = \sqrt{\frac{24H^2(1-\nu)\sigma^3}{Yr^2}(1-\frac{\sigma_R}{\sigma})} \tag{5-3}$$

In order to have a X-ray window that can withstand a pressure differential of 1 atm made of LSSN with a freestanding circular geometry and a diameter of 7 mm with values for Young's modulus, residual stress and tensile strength found during the characterization (figure 5-1 $Y =$ 2.26 x 10^{11} Pa $\sigma_R =$ 1.41 x 10^8 Pa, $\sigma_T =$ 8.74 x 10^8 Pa), the thickness of the film would need to be 1.7 microns. The X-ray transmission for this window would be much worse than the 8 micron beryllium windows as is shown in figure 5-1.

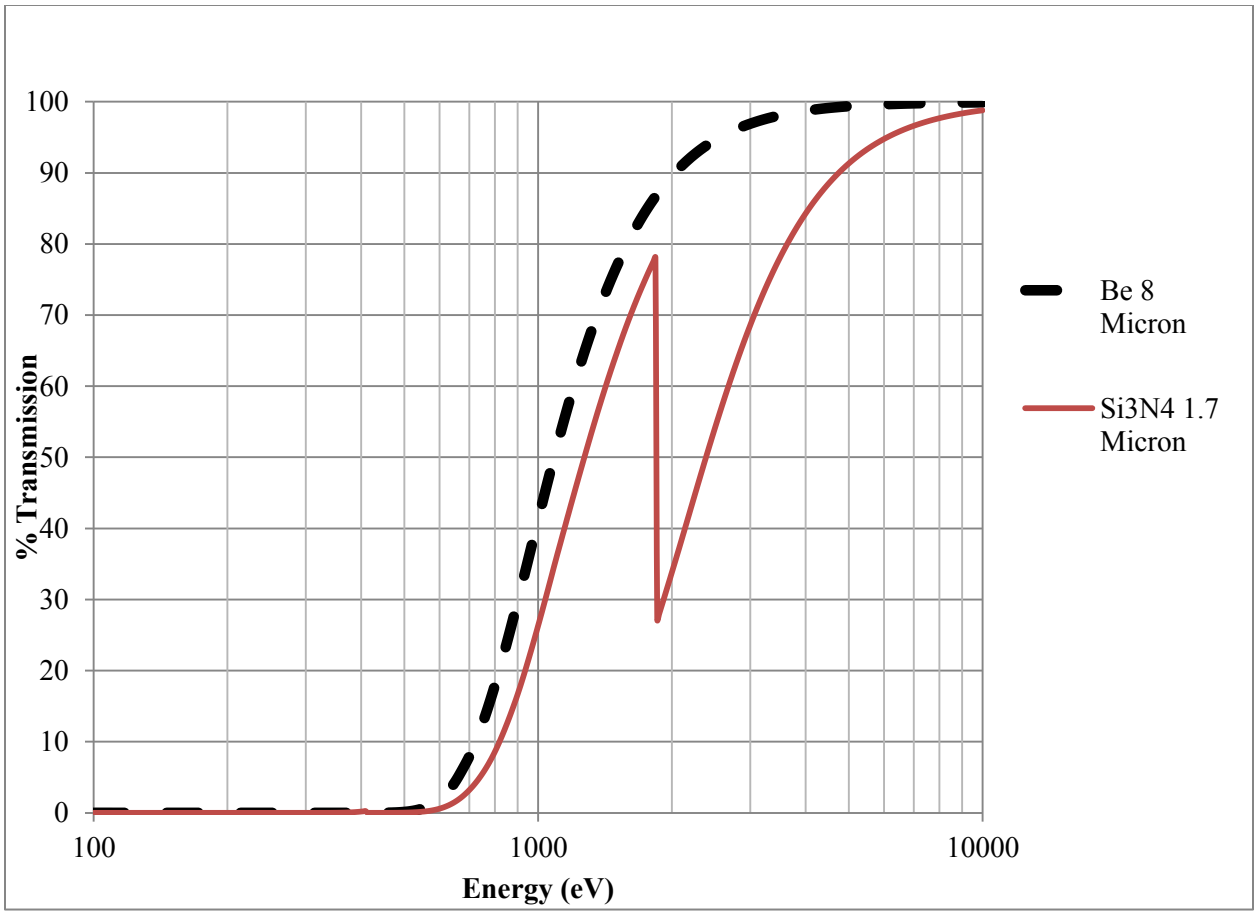

Figure 5-1 X-ray transmission curves for freestanding 8 micron beryllium and 1.7 micron silicon nitride

Using equation 5-3 and the same characterized materials parameters used to create the plot in figure 5-1, the residual stress of a LSSN would have to be compressive and have a magnitude of 2.4 MPa in order to have the film with a thickness of 600 nm be able to withstand 1 atm of pressure in the freestanding geometry. A LSSN film with the freestanding geometry with a residual stress greater than -2.4 MPa is mechanically stable enough to function as a suitable X-ray window material with a thickness that would allow for X-ray transmission comparable to 8 micron beryllium windows.

As mentioned earlier in section 3.9, the tensile strength of the material found in this experiment (and the value used in the calculation above, 8.74×10^8 Pa) is one order of magnitude

less than the values reported in the literature. If the LSSN had a tensile strength of 5 x 10^9 Pa, the thickness required to withstand 1 atm of pressure with the freestanding circular geometry with a 7 mm diameter is roughly 100 nm. If the LSSN could be fabricated with a tensile strength close to values reported in the literature, the window could be made with a thickness that would allow for X-ray transmission similar to 8 micron thick beryllium X-ray windows. Such a window may be a possible replacement material for beryllium.

5.2 X-ray Window Resonance Frequencies

The fundamental frequencies of thin-films need to be calculated in order to better understand their response to mechanical shock wave. If the frequencies found in the shock wave are below the fundamental frequency of the film, the effect the mechanical shock has on the film will be very different than if the shock wave can excite standing waves in the thin film.

The fundamental frequencies for a circular membrane with the freestanding geometry made from LSSN and beryllium were calculated using equation 5-4. The derivation of equation 5-4 can be found in Appendix E. The first five resonance frequencies can be found on figure 5-4.

$$f_n = \frac{j_n c}{2\pi r} \tag{5-4}$$

In equation 5-4 j_n are the zeros for the Zeroth Order Bessel Function, c is the speed of sound in a material, and r is the radius of the membrane. Assuming that the membrane is made from a material that is isotropic and homogenous, the speed of sound in the material can be calculated using the Young's modulus Y, Poisson's ratio ν and mass density ρ as shown in equation 5-5 [32].

$$c = \sqrt{\frac{Y(1-\nu)}{\rho(1-2\nu)(1+\nu)}} \tag{5-5}$$

The first five calculated frequencies for membranes made from beryllium and LSSN can be found on table 5-1 ($v = 0.25$, $\rho = 3.0$ g/cm^3, $Y = 2 \times 10^{11}$ Pa, $r = 3.5 \times 10^{-3}$ m).

Beryllium (Hz)	Low Stress Silicon Nitride (Hz)
1.36×10^6	**9.76×10^5**
3.12×10^6	**2.24×10^6**
4.90×10^6	**3.52×10^6**
6.68×10^6	**4.80×10^6**
8.46×10^6	**6.07×10^6**

Table 5-1 The first five resonance requances for low stress silicon nitride and beryllium with freestanding circular geometry

The bandwidth for the accelerometer used is 0.2 Hz to 25 kHz. All of the resonance frequencies are well above 25 kHz and therefore could not be measured. An example of a typical mechanical shock wave created by the pendulum shock apparatus can be found in figure 5-2.

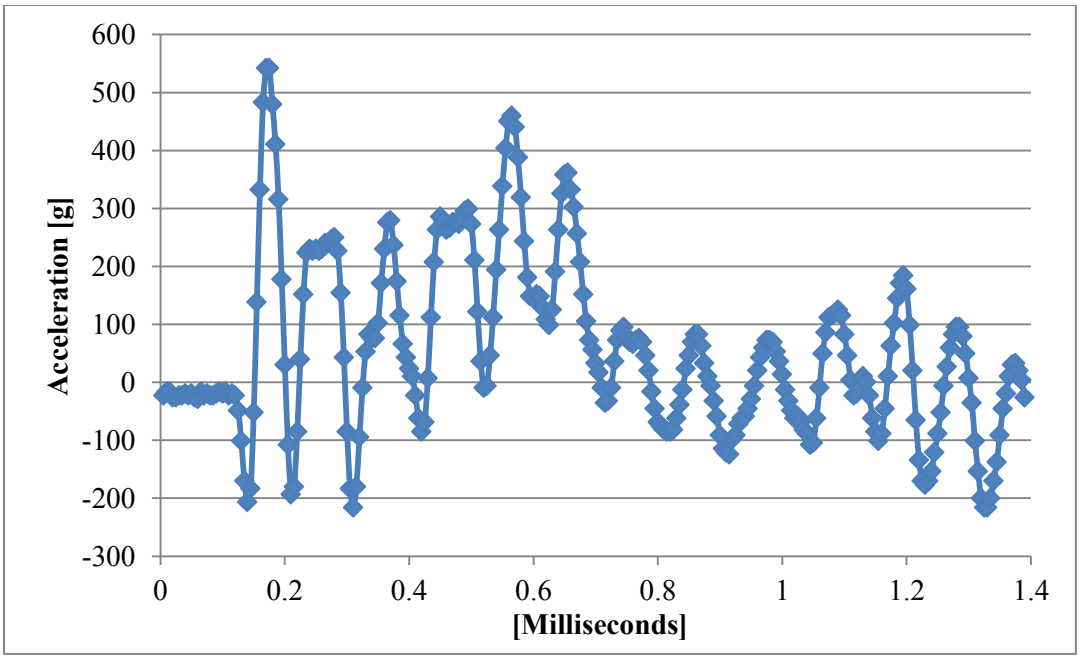

Figure 5-2 Acceleration measurement of mechanical shock wave created by pendulum shock apparatus.

All mechanical shock waves showed a maximum acceleration at either the first or second crest. A Fourier transform of mechanical shock waves showed that the dominate frequencies were in the 10^3 Hz and 10^4 Hz range as shown in figure 5-3. This frequency range is must less than the resonance frequencies, which means that the shock is likely not exciting any vibrations modes in the films.

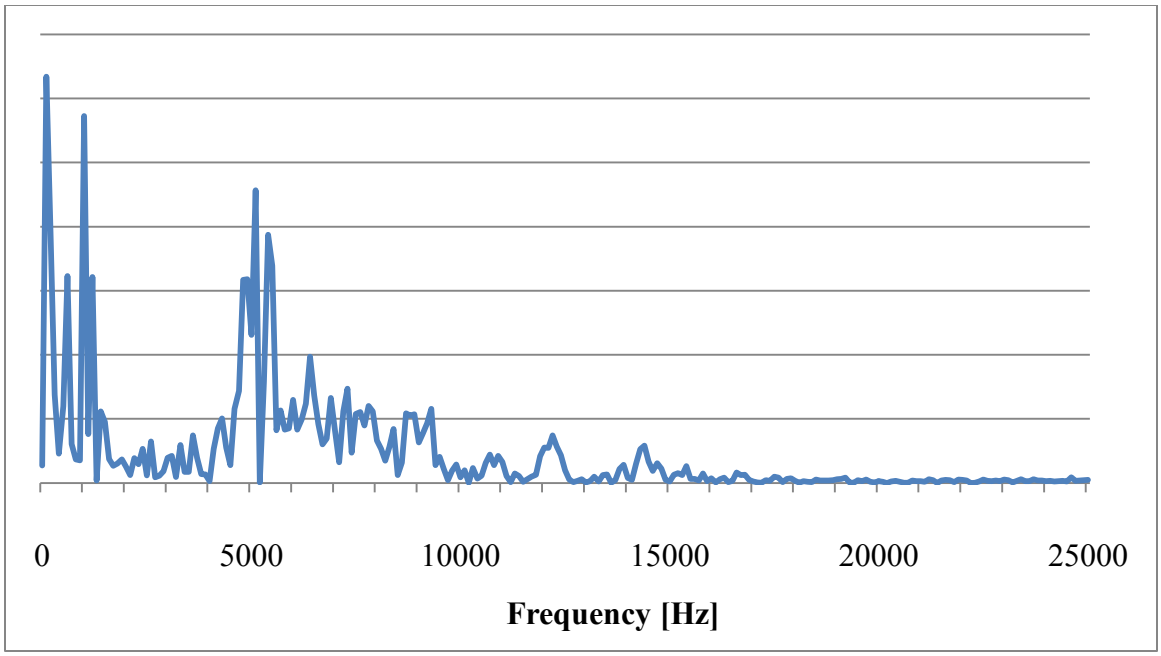

Figure 5-3 Fourier transfor spectrum of mechanical shock wave. The dominate frequencies are in the 10^3 to 10^4 range.

5.3 Quasistatic Shock Pressure Approximation

Because the resonance frequencies of the film are much higher than the frequencies caused by mechanical shock, wave freestanding waves in the thin film will not be excited and the shock stress will be modeled with a quasistatic approximation using an effective "shock pressure" due to acceleration. All vibration modes will be ignored. Using this approximation, the acceleration required to break a 635 nm thick LSSN membrane is 10^6 g. The following section outlines the approximation and subsequent equations and calculation.

Assuming that shock pressure, $P_{s,}$ is isotropic and that the membrane is isotropic and homogenous, the acceleration and the shock pressure can be related to one another as shown in equation 5-6.

$$P_s = \frac{F}{A} = \frac{g\rho V}{A} = \frac{g\rho H\pi r^2}{\pi r^2} = g\rho H \qquad (5\text{-}6)$$

In equation 5-6, g is the acceleration, ρ is the density of the material and H is the thickness of the membrane. By substituting in the shock pressure for the pressure found in equation 5-3, a relationship between acceleration and stress on the membrane can be found as shown in equation 5-7.

$$g = \sqrt{\frac{24(1-\nu)\sigma^3}{Y\rho^2 r^2}\left(1-\frac{\sigma_R}{\sigma}\right)} \qquad (5\text{-}7)$$

Equation 5-7 relates acceleration, g, to stress and can be used to determine the stress caused by a given acceleration during a shock wave. In order to compare the stress caused by both acceleration and pressure, the plots in figures 5-4 and 5-5 were created for an idealized LSSN film with zero residual stress. The values for r, H, and Y were found experimentally, and ν and ρ were found in the literature ($Y = 2.26 \times 10^{11}$ Pa $r = 3.5 \times 10^{-3}$ m, $\nu = 0.25$, $H = 635 \times 10^{-9}$ m, and $\rho = 3000$ kg/m^3) [28] [40].

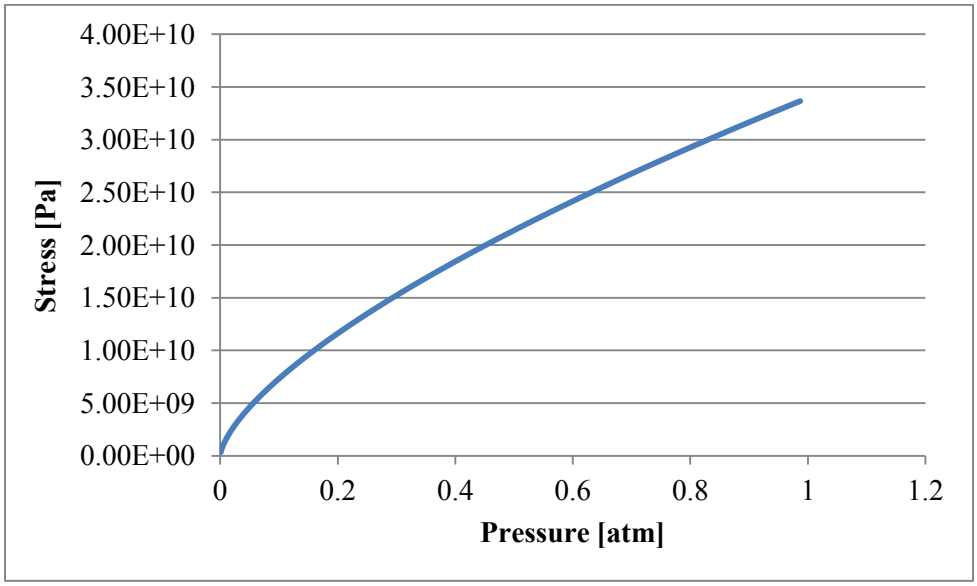

Figure 5-4 A plot of equation 5-8 with a low stress silicon nitride film with no residual stress in the freestanding geometry.

Figures 5-4 and 5-5 are plots of pressure vs. stress and acceleration vs. stress on a LSSN film with no residual stress using equations 5-5 and 5-7 respectively. According to equation 5-7, the acceleration required to fracture a 635 nm thick LSSN films with the freestanding geometry is 10^6 g. This means that acceleration due to a shock will likely not cause a thin film to rupture under normal circumstances. There are experimental results to support this. The LSSN films with a freestanding geometry were shock tested without an applied vacuum and were able to

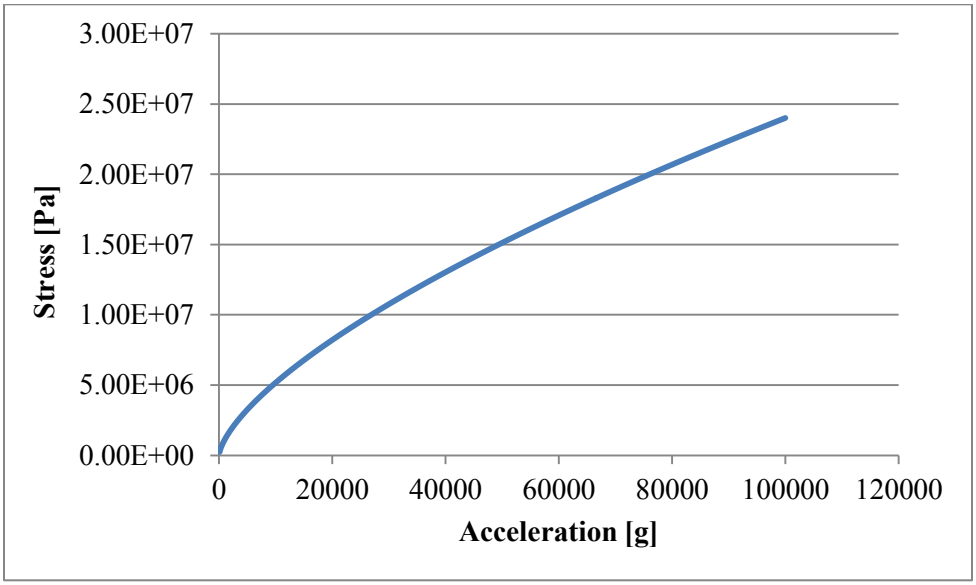

Figure 5-5 A plot of stress veres acceleration using equation 5-7 for a low stress silicon nitride film with no residual stress in a freestanding circular geometry.

withstand accelerations of up to 10^5 g without fracturing (see figure 4-7). The support structure windows were shock tested with an applied vacuum and fractured with accelerations of 10^4 g. Yet the freestanding geometry was not able to withstand the stress to hold an atmosphere of pressure, and the support structure windows were. These results show that for a freestanding circular geometry, an applied vacuum causes more stress on the X-ray windows than accelerations caused by the mechanical shock wave. Similar pressure and acceleration vs. stress

graphs for the support structure LSSN windows cannot be modeled using equations 5-5 and 5-7 because of the complex geometry.

For future work there are two main objectives that should be considered. One objective is to characterize the residual stress in the low stress silicon nitride. By minimizing the residual stress, a large applied stress can be applied before reaching the tensile strength of the material.

The second objective is to determine if the LSSN films that were fabricated do have a tensile stress that is one order of magnitude lower than the values reported in the literature, or if the calculated values are incorrect. Perhaps another method could be used to verify the materials tensile strength.

Chapter 6

Summary and Conclusions

6.1 X-ray Windows Comparison

	Beryllium Window	**100 nm LSSN Support Structure**	**200 nm LSSN Support Structure**	**600 nm Freestanding LSSN**
Shock Test	**>30,000 g**	**5,000-3,300 g**	**6,000-5,000 g**	**>12,000 g**
Burst Test	**>2 atm**	**1.4 atm**	**2.2 atm**	**0.4 atm**
Cycling	**>100**	**>100**	**>100**	**NA**
Max Allowed Leak Rate	**$<3 \times 10^{-9}$ mbar-L/s**	**$<3 \times 10^{-9}$ mbar-L/s**	**$<3 \times 10^{-9}$ mbar-L/s**	**NA**
Open Area	**100%**	**77%**	**77%**	**100%**

Table 6-1 Overall Comparison of X-ray Window Materials

Several observations can be made by comparing the window testing results of the LSSN windows in both geometries and the information available for 8 micron beryllium windows provided by its specification sheet. The support structure LSSN window had superior X-ray transmission at low energies compared to the freestanding 600 nm thick LSSN and 8 micron thick beryllium X-ray windows. They also showed reasonable mechanical shock resistivity with an applied vacuum. Based on the drop height acceleration characterization, the 200 nm support structure LSSN window can withstand being dropped from a height of just over 3 ft. without

failing. Also the 200 nm thick support structure windows were the only windows that met the same burst pressure specification as 8 micron beryllium windows.

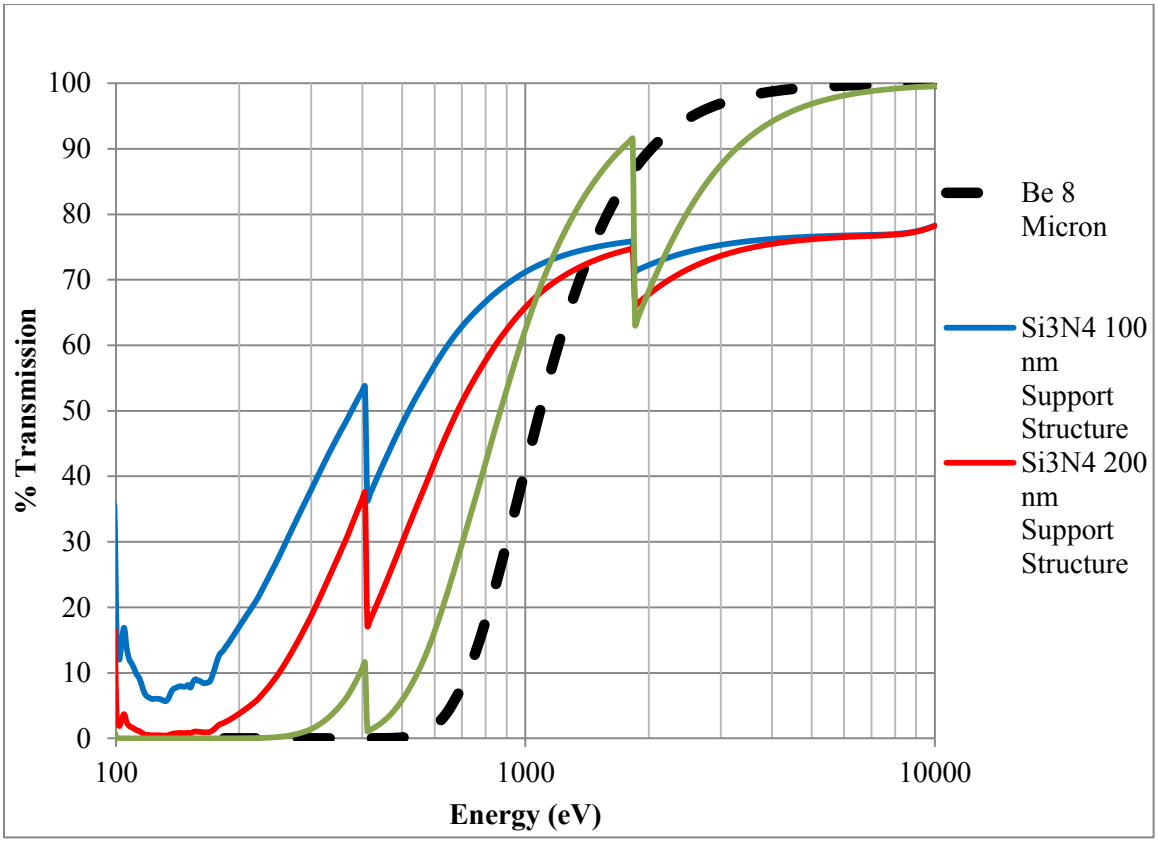

Figure 6-1 X-ray transmission curves for tested windows

6.2 Future Work

LSSN may potentially be a replacement material for beryllium, but only with a support structure. The residual stress and support structure geometry would need to be optimized. Residual stress has been shown to depend on deposition pressure, temperature and input gas ratio (SCl_2H_2/NH_3) [2] [23] [27]. A film with lower residual stress will be able to withstand a higher pressure difference before bursting for the same geometry. Therefore a film can span a greater distance without failing under the required pressure conditions with a lower residual stress.

Once the residual stress has been optimized, the support structure will also need to be optimized. The transfer of the LSSN films to Al washers shows that the film can be transferred to any given geometry and material. A support structure made from low Z elements with a large open area could be used and create a window made for non-toxic LSSN that has similar X-ray transmission to 8 micron beryllium windows.

Appendix A

Relationship between Pressure and Stress for a Suspended Thin-Film

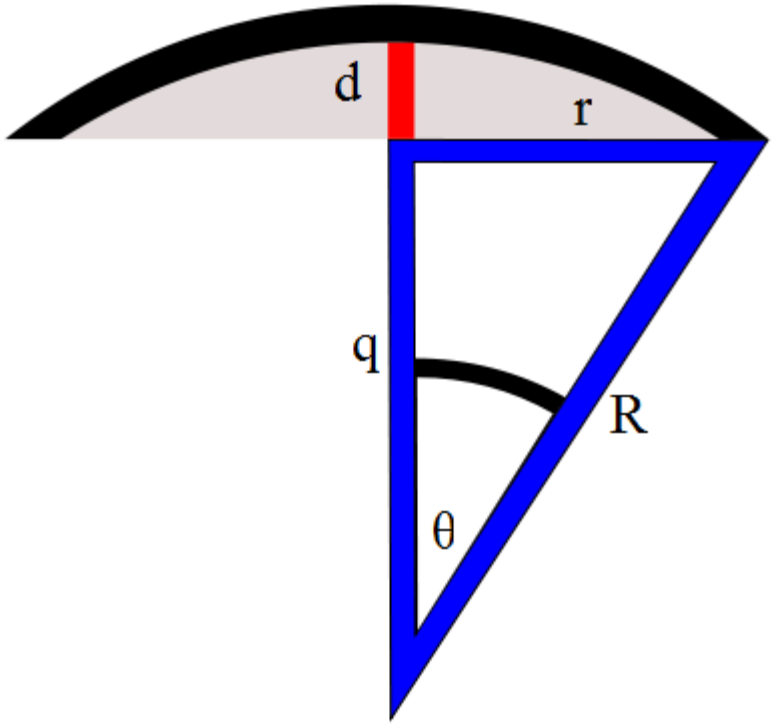

Figure A-1 A visualization of the relationships between R, q, r, h and θ.

Assuming spherical geometry, the two definitions of R are found below in equations A-1 and A-2 as shown in figure A-1.

$$R = q + d \qquad \text{(A-1)}$$

$$R^2 = q^2 + r^2 \qquad \text{(A-2)}$$

We can eliminate the parameter q by substitution and define R interns of the deflection of the membrane, d, and the radius of the thin film, r. The result can be simplified in the case where we have small deflections ($r>>d$) as shown in equation A-3.

$$R = \frac{d}{2} + \frac{r^2}{2d} \cong \frac{r^2}{2d} \tag{A-3}$$

This approximation for *R* will be used later in the derivation.

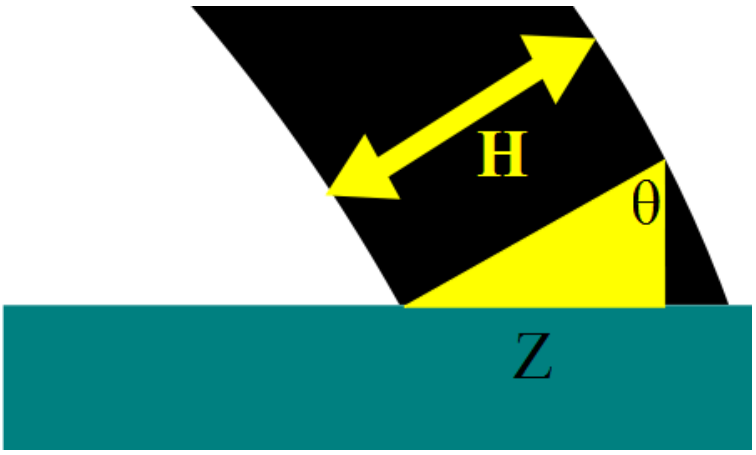

Figure A-2 Avisualization of the relationships between H, Z and θ

Because the film is in static equilibrium, equation A-4 must be satisfied.

$$F_{down} = F_{up} \tag{A-4}$$

The force in the downward direction is due to the stress in the film and the force in the upward direction is due to the pressure. The stress times the area is equal to the force in the downward direction as shown in equation A-5. (It should be noted that the maximum strain of the LSSN films caused by the applied pressure during bulge testing for our experiment is on the order of 10^{-3}. As a result, an approximation is made that the thickness, *H,* is constant.)

$$F_{down} = \sigma A = \sigma 2\pi r Z = 2\pi r H \sigma sin\theta \tag{A-5}$$

The force in the upward direction is equal to the pressure times the area as described in equation A-6.

$$F_{up} = PA = P\pi r^2 \tag{A-6}$$

By equating the force in the upward direction to the force in the downward direction, we get the following equation.

$$P\pi r^2 = 2\pi r H \sigma sin\theta \tag{A-7}$$

After some algebraic massaging and using the relationship found in equation A-8, an expression for pressure as a function of the film thickness, *H*, deflection, *d*, stress, σ and radius of the film, *r*, can be found as shown in equation A-9.

$$sin\theta = \frac{r}{R} \tag{A-8}$$

$$P = \frac{2H\sigma}{R} \cong \frac{4Hd\sigma}{r^2} \tag{A-9}$$

Appendix B

Biaxial Hook's Law

In an isotropic material, stress can be related to strain in the same direction using the scalar form of Hook's Law as shown in equation B-1.

$$\sigma_i = Y\varepsilon_i \tag{B-1}$$

In equation B-1, σ is the stress, Y is the Young's modulus, and ε is the strain. The strain in the direction perpendicular to the stress in an isotropic material can be described using equation B-2.

$$\sigma_i = -\frac{Y}{\nu}\varepsilon_j \tag{B-2}$$

In equation B-2 ν is the Poisson's ratio of the material and all of the other variables are the same as defined in equation B-1.

A matrix representation relating the strain to the stress can be found in equation B-3.

$$\varepsilon_i = \frac{1}{Y}\left[\delta_{ij}(1+\nu) - \nu\right]\sigma_j \tag{B-3}$$

In the case where the strains is equal in two of the directions and zero in the other the matrix takes the following form.

$$\begin{bmatrix}\varepsilon_1\\ \varepsilon_2\\ \varepsilon_3\end{bmatrix} = \frac{1}{Y}\begin{bmatrix}1 & -\nu & -\nu\\ -\nu & 1 & -\nu\\ -\nu & -\nu & 1\end{bmatrix}\begin{bmatrix}\sigma\\ \sigma\\ 0\end{bmatrix} \tag{B-4}$$

ε_1 and ε_2 are equal to each another and are the biaxial Hook's law equation as shown in equation B-5.

$$\sigma = \frac{Y}{1-\nu}\varepsilon \tag{B-5}$$

Appendix C

Strain as a Function of Film Deflection

Strain is defined as a change in length divided by the initial length. In the case of strain on a thin film due to pressure, the strain can be related to the arc length of the film as show in equation C-1.

$$\varepsilon = \frac{\Delta l}{l} = \frac{\Delta(R\theta)}{R\theta} \tag{C-1}$$

θ can be related to the arcsine of r and R and with the small deflection approximation to a Taylor series expansion as shown in equation C-2.

$$\theta = \arcsin\left(\frac{r}{R}\right) \cong \frac{r}{R} + \frac{r^3}{6R^3} \tag{C-2}$$

Using equation C-2 and the approximation of R in equation A-3, the strain can be approximated by equation C-3.

$$\varepsilon = \frac{\Delta(R\theta)}{R\theta} = \frac{r + \frac{2(d_i + \Delta d)^2}{3r} - \left(r + \frac{2d_i^2}{3r}\right)}{r + \frac{2d_i^2}{3r}}$$

$$\varepsilon = \frac{\frac{2}{3r}(2d_i\Delta d + (\Delta d)^2)}{r + \frac{2d_i^2}{3r}} \tag{C-3}$$

If the initial deflection is assumed to be zero ($d_i = 0$), then the approximation for the strain can be reduced further as shown in equation C-4.

$$\varepsilon \cong \frac{2d^2}{3r^2} \tag{C-4}$$

Equation C-4 gives the relationship between the strain on thin-films due to the deflection of the thin film for small deflections.

Appendix D

Derivation of the Bulge Equation

Starting from the biaxial stress and strain relation found in equation B-5 and substituting in the approximation for stress and strain found in equations A-9 and C-4 respectively the following relationship can be found.

$$\frac{Pr^2}{4Hd} = \frac{Y}{1-\nu}\frac{2d^2}{3r^2} \tag{D-1}$$

The term on the left had side of the equation represents all of the stress in the film. In order to account for the residual stress in the film, a residual stress term, σ_R, is added to equation D-1. The equation is then solved for P. The resulting equation is the bulge equation.

$$P = \frac{4Hd}{r^2}\left[\sigma_R + \frac{2d^2Y}{3r^2(1-\nu)}\right] \tag{D-2}$$

Appendix E

Membrane Vibration Frequencies

The wave equation and the general form of the solution can be found in equations E-1 and E-2.

$$\nabla^2 \xi = \frac{1}{c^2}\frac{\partial^2 \xi}{\partial t^2} \tag{E-1}$$

$$\xi = \psi e^{i\omega t} \tag{E-2}$$

In equation E-1, c is the speed of the wave. In equation E-2, ψ is a function of only position and varies based on boundary conditions [30]. The solution for a circular vibrating membrane on fixed rim can be found in equation E-3.

$$\xi(r,\theta,t) = A_{mn} J_m(k_{mn} r)\cos(m\theta + \phi_{mn}) e^{i\omega_{mn} t} \tag{E-3}$$

A_{mn}, k_{mn}, φ_{mn}, and m are constants that can be found using boundary conditions. $J_m(k_{mn}r)$ are Bessel functions of order m. If azimuthal symmetry can be assumed, the solution reduces to a function of only radius and time and shown in equation E-4.

$$\xi(r,t) = A_n J_o(k_n r) e^{i\omega_n t} \tag{E-4}$$

J_o is Bessel function of order zero, and k_n can be determined using equation E-5. The fundamental frequencies of the membrane can be found by using equation E-6.

$$k_n = \frac{j_n}{a} \tag{E-5}$$

$$f_n = \frac{j_n c}{2\pi a} \tag{E-6}$$

In equation E-5, j_n are the zeros of J_o. In equation E-6, c is the speed of the wave and a is the radius of the circle [31].

Bibliography

[1]. M.Ohing, *Materials Science of Thin Films Deposition and Structure*, 2nd ed. (Academic Press, San Diego, 2002) p. 610.

[2]. M. Sekimoto, H. Yoshihara, and T. Ohkubo, J. Vac. Sci. Technol., "Silicon nitride single-layer X-ray mask," 21, 1017-1021 (4), (1982).

[3]. NASA, FS-2000-07-159-MSFC, August, (2000).

[4]. B. L. Henke, E. M. Gullikson, and J. C. Davis, "X-Ray Interactions: Photoabsorption, Scattering, Transmission, and Reflection at E=50-30,000 eV, Z= 1-92," Atomic Data and Nuclear Data Tables, 54 (2), 181-342, (1993).

[5]. M.Ohing, *Materials Science of Thin Films Deposition and Structure*, 2nd ed. (Academic Press, San Diego, 2002) p. 730.

[6]. P.J. French, P. M. Sarro, R. Mallee, E. J. M. Fakkeldij, and R. F. Wolffenbuttel, "Optimization of low-stress silicon nitride process for surface-micromachining applications", Sens. And Actuat. A 58, 149-157 (1997).

[7]. M.Ohing, *Materials Science of Thin Films Deposition and Structure*, 2nd ed. (Academic Press, San Diego, 2002) p. 317.

[8]. M.Ohing, *Materials Science of Thin Films Deposition and Structure*, 2nd ed. (Academic Press, San Diego, 2002) p. 306.

[9]. M. J. Madou, *Fundamentals of Microfabrication The Science of Miniaturization*, 2nd ed. (CRC Press, New York) p. 6.

[10]. M. J. Madou, *Fundamentals of Microfabrication The Science of Miniaturization*, 2nd ed. (CRC Press, New York) p. 4.

[11]. M. J. Madou, *Fundamentals of Microfabrication The Science of Miniaturization*, 2nd ed. (CRC Press, New York) p. 101.

[12]. M. J. Madou, *Fundamentals of Microfabrication The Science of Miniaturization*, 2nd ed. (CRC Press, New York) p. 216.

[13] J. H. Hubbell, W. J. Veigele, E. A. Briggs, R. T. Brown, D. T. Cromer, and R. J. Howerton, "Atomic Form Factors, Incoherent Scattering Functions, and Photon Scattering Cross Sections," J. Phys. Chem. Ref. Data 4, 471-538 (1975).

[14] J. Allyn, "Correlation Between Electrical Pulse Resistance and Mechanical Shock Resistance for Four Casting Resins" Annual Report, Sandia Corporation, 96-98, (1964).

[15] D. Reiff, E. Bradley, "A Novel Mechanical Shock Test Method to Evaluate Lead-Free BGA Solder Joint Reliability" Electronic Components and Technology Conference, 1519-1525, (2005).

[16] J. Pitarresi, B. Roggenman, S. Chaparala, "Mechanical Shock Testing and Modeling of PC Motherboards", Electronic Components and Technology Conference, 1047-1054, (2004).

[17] E. Suhir, "Could Shock Tests Adequately Mimic Drop Test Conditions?", J. Electro. Packaging, 124, 3, 170-177, (2002).

[18] P.F. Infante, L. S. Newman, "Beryllium Exposure and Chronic Beryllium Disease," Lancet, 363, 9407, 415-416, (2004).

[19] J. Emsley, *Nature's Building Blocks: An A-Z Guide to the Elements*, Oxford, England, Oxford University Press, (2001).

[20] World Health Organization, *Beryllium Health and Safety Guide*, World Health Organization for International Programme on Chemical Safety 44. (1990).

[21] R. Rimback, A. J. Michel, *Beryllium Its Production and Application,* Zentralstelle Für Wissenschaftlich-Technische Siemens-Konzerns Firm, (1932).

[22] R. Mutikainen, S. Nenonen, V. Viitanen, "Grid Supported Polyimide and Beryllium Based Soft X-ray Windows – Pressurized Membrane Ductility Considerations" M. Nastasi et al. (eds.), Mechanical Properties and Deformation Behavior of Materials Having Ultra-Fine Microstructures, 337-342, Kluwer Academic Publishers, 1993.

[23] Y. Toivola, J. Thurn, R. F. Cook, G. Cibuzar, K. Roberts, "Influence of deposition conditions on mechanical properties of low-pressure chemical vapor deposited low-stress silicon nitride films", J. App. Phys., 94,10, (2003).

[24] J. Knapp, E. Altmann, J. Niemann, K. D. Werner, "Measurement of shock events by means of strain gauges and accelerometers," Measurement, 24, 2, 87-96, (1998).

[25] T. Ebata, M. Sekimoto, T Ono, K. Suzuki, J. Matsui, and S. Nakayama, "Transparent X-Ray Lithography Masks," Japanese Journal of Applied Physics, 21, 5, 762-767, (1982).

[26] S. Timoshenko and S. Woinowsky-Krieger, "Theory of Plates and Shells", 2nd Ed. (New York, McGraw-Hill, p. 419-420.

[27]. R. Ghodssi, P. Lin, *MEMS Materials and Processes Handbook*, (Springer, New York, 2011) p. 71.

[28] W. Chuang, T. Lugar, R. K. Fettig, R. Ghodssi, "Mechanical Property Characterization of LPCVD Silicon Nitride Films at Cryogenic Temperatures", Journal of Microelectromechanical Systems, 13, 5, 870-879, (2004)

[29] J. J. Vlassak, W. D. Nix, "New Bulge Test Technique for the Determination of Young's Modulus and Poisson's Ratio of Thin Films", Journal of Material Research, 7, 12, 3242-3249, (1992).

[30]. L. E. Kinsler, A. R. Frey, A. B. Coppens, J. V. Sanders, *Fundamentals of Acoustics*, 4th ed. (John Wiley and Sons Inc., New York) p. 93.

[31] L. E. Kinsler, A. R. Frey, A. B. Coppens, J. V. Sanders, *Fundamentals of Acoustics*, 4th ed. (John Wiley and Sons Inc., New York) p. 97.

[32] L. E. Kinsler, A. R. Frey, A. B. Coppens, J. V. Sanders, *Fundamentals of Acoustics*, 4th ed. (John Wiley and Sons Inc., New York) p. 160.

[33] G. Arfken, *Mathematical Methods for Physicists*, 3th ed. (Academic Press, Orlando) p. 787.

[34] F. S. Tsai, "Characterization of Mechanical and Optical Properties of X-ray Mask Membranes", Thesis, MIT (1991).

[35] G. M. Owen, "Optical and Mechanical Characterization of Thin Membranes for X-ray Lithography", Thesis, MIT (1994).

[36] G. C. Stoney, Proc. Roy. Soc. London., A32, 172, (1909).

[37] Personal communication with Jonathan Abbott, Moxtek Inc.

[38] C. Wu, W. Fang, M. Yip, "Measurement of Mechanical Properties of Thin Films Using Bulge Test", Soc. Exp. Mech. Proc., 22, p 5, (2004).

[39] R. Wyman, "Bulge Testing of Duracoat and Carbon in Large Deflection Limit", Senior Thesis, Department of Physics and Astronomy Brigham Young University (2012) .

[40] C. H. Mastrangelo, Y. Tai, R. S. Muller, "Thermophysical Properties of Low-residual Stress, Silicon-rich, LPCVD, Silicon Nitride Films", Sensors and Actuators, A21-A23, 856-860, (1990).

[41] K. E. Petersen, "Silicon as a Mechanical Material," Procee. Of the IEEE, 70, 5, (1982).

[42] E. A. Irene, "Residual Stress in Silicon Nitride Films", Journal of Electronic Materials, Vol. 5, 3, (1976)

[43] The Center for X-ray Optics website.

[44] J. J. Wortman, R. A. Evans, “Young’s Modulus, Shear Modulus, and Poisson’s Ratio in Silicon and Germanium, J. Appl. Phy. 36, 153 (1965)

[45] M. A. Hocroft, W. D. Nix, T. W. Kenny, “What is the Young’s Modulus of Silicon?”, J. Microelectromechanical Sys. 19, 2, 229-238, (2010)

[46] A. Kaushik, H. Kahn, A. H. Heuer, “Wafer-Level Mechanical Characterization of Silicon Nitirde MEMS”, J. Microelectromechanical Sys. 14, 2, 359-367, (2005)